National Library of Canada

Bibliothèque nationale du Canada

Acquisitions and Bibliographic Services Branch

Direction des acquisitions et des services bibliographiques

395 Wellington Street
Ottawa, Ontario
K1A 0N4

395, rue Wellington
Ottawa (Ontario)
K1A 0N4

Your file Votre référence

Our file Notre référence

NOTICE

The quality of this microform is heavily dependent upon the quality of the original thesis submitted for microfilming. Every effort has been made to ensure the highest quality of reproduction possible.

If pages are missing, contact the university which granted the degree.

Some pages may have indistinct print especially if the original pages were typed with a poor typewriter ribbon or if the university sent us an inferior photocopy.

Reproduction in full or in part of this microform is governed by the Canadian Copyright Act, R.S.C. 1970, c. C-30, and subsequent amendments.

AVIS

La qualité de cette microforme dépend grandement de la qualité de la thèse soumise au microfilmage. Nous avons tout fait pour assurer une qualité supérieure de reproduction.

S'il manque des pages, veuillez communiquer avec l'université qui a conféré le grade.

La qualité d'impression de certaines pages peut laisser à désirer, surtout si les pages originales ont été dactylographiées à l'aide d'un ruban usé ou si l'université nous a fait parvenir une photocopie de qualité inférieure.

La reproduction, même partielle, de cette microforme est soumise à la Loi canadienne sur le droit d'auteur, SRC 1970, c. C-30, et ses amendements subséquents.

Canada

The Study of Restacked Single Molecular Layer Molybdenum Disulfide with Organic Tetrachloroethylene Included

by

Xinyan Zhou
B.Sc., Sichuan Normal University, 1984

THESIS SUBMITTED IN PARTIAL FULFILLMENT OF

THE REQUIREMENTS FOR THE DEGREE OF

MASTER OF SCIENCE

in the Department

of

Physics

© Xinyan Zhou 1994

SIMON FRASER UNIVERSITY

NOVEMBER, 1994

All rights reserved. This work may not be
reproduced in whole or in part, by photocopy
or other means, without permission of the author.

National Library of Canada

Bibliothèque nationale du Canada

Acquisitions and Bibliographic Services Branch

Direction des acquisitions et des services bibliographiques

395 Wellington Street
Ottawa, Ontario
K1A 0N4

395, rue Wellington
Ottawa (Ontario)
K1A 0N4

Your file Votre référence

Our file Notre référence

THE AUTHOR HAS GRANTED AN IRREVOCABLE NON-EXCLUSIVE LICENCE ALLOWING THE NATIONAL LIBRARY OF CANADA TO REPRODUCE, LOAN, DISTRIBUTE OR SELL COPIES OF HIS/HER THESIS BY ANY MEANS AND IN ANY FORM OR FORMAT, MAKING THIS THESIS AVAILABLE TO INTERESTED PERSONS.

L'AUTEUR A ACCORDE UNE LICENCE IRREVOCABLE ET NON EXCLUSIVE PERMETTANT A LA BIBLIOTHEQUE NATIONALE DU CANADA DE REPRODUIRE, PRETER, DISTRIBUER OU VENDRE DES COPIES DE SA THESE DE QUELQUE MANIERE ET SOUS QUELQUE FORME QUE CE SOIT POUR METTRE DES EXEMPLAIRES DE CETTE THESE A LA DISPOSITION DES PERSONNE INTERESSEES.

THE AUTHOR RETAINS OWNERSHIP OF THE COPYRIGHT IN HIS/HER THESIS. NEITHER THE THESIS NOR SUBSTANTIAL EXTRACTS FROM IT MAY BE PRINTED OR OTHERWISE REPRODUCED WITHOUT HIS/HER PERMISSION.

L'AUTEUR CONSERVE LA PROPRIETE DU DROIT D'AUTEUR QUI PROTEGE SA THESE. NI LA THESE NI DES EXTRAITS SUBSTANTIELS DE CELLE-CI NE DOIVENT ETRE IMPRIMES OU AUTREMENT REPRODUITS SANS SON AUTORISATION.

ISBN 0-612-06886-2

Canadä

APPROVAL

Name: Xinyan Zhou

Degree: Master of Science (Physics)

Title of Thesis: The Study of Restacked Single Molecular Layer Molybdenum disulfide with Organic Tetrachloroethylene Included

Examining Committee:

Chair: Barbara Frisken

Robert F. Frindt
Senior Supervisor
Professor of Physics

Albert Curzon
Professor of Physics

E. Daryl Crozier
Professor of Physics

Jeff Dahn
Internal Examiner
Professor of Physics

Date Approved: 30 November 94

PARTIAL COPYRIGHT LICENSE

I hereby grant to Simon Fraser University the right to lend my thesis, project or extended essay (the title of which is shown below) to users of the Simon Fraser University Library, and to make partial or single copies only for such users or in response to a request from the library of any other university, or other educational institution, on its own behalf or for one of its users. I further agree that permission for multiple copying of this work for scholarly purposes may be granted by me or the Dean of Graduate Studies. It is understood that copying or publication of this work for financial gain shall not be allowed without my written permission.

Title of Thesis/Project/Extended Essay

The Study of Restacked Single Molecular Layer Molybdenum Disulfide with

Organic Tetrachloroethylene Included

Author: ____________________
(signature)

Xinyan Zhou
(name)

13 December 1994
(date)

Abstract

The structure of restacked monomolecular layers of MoS_2 with organic tetrachloroethylene (TCE) included was studied using X-ray powder diffraction and X-ray diffraction of thin films in reflection and transmission. It was found that the MoS_2 host layers are separated by a monolayer of TCE and that the MoS_2 is strongly distorted, with the Mo in an octahedral coordination.

Optical absorption and electrical resistance measurements were performed on the MoS_2/TCE system. The results support the conclusion drawn from the X-ray studies that the MoS_2 in the MoS_2/TCE system exhibits properties similar to those for the MoS_2/water bilayer system. A 15K resistive transition observed by other workers for MoS_2/poly-ethylene-oxide (PEO) is not observed in the MoS_2/TCE system.

Acknowledgments

I wish to express my deepest gratitude to my senior supervisor Dr. R. F. Frindt for his guidance, support and questions posed, the relevance of which I eventually learned to appreciate.

Special thanks are due to Dr. D. Yang who shared with me the knowledge and lab skills he accumulated over years. I am grateful to him for all the help and advice I received from him throughout this project.

Many thanks are due to Dr. A. Curzon and Dr. E. D. Crozier who carefully read through my thesis and gave me lots of valuable suggestions. I wish to thank Dr. E. D. Crozier also for suggesting and providing to me the sample substrate used in the X-ray transmission measurements.

I also enjoyed the positive discussions with Dr. J. Dahn, his advice and his supportive attitude toward my using the experimental facilities in his lab.

I wish to thank my fellow students who have enlighten me through various discussions. Among them are Brian Way, Tao Zheng, Kevin Hewitt, Jinsheng Hu and Yubo Yang.

I would like to thank Ms. Sue Zhang and Ms. Meihua Gao in Chemistry Department for their assistance in the optical absorption experiment.

The support from the department technicians, Mike Billany and Scott Wilson, is also appreciated. I thank Dr. S. S. Rangnekar, Shauna Smith-Simpson, Sharon Beever, Andrey Reid and Julia MacAdam for their help in dealing with the paper work. I thank the Thesis Assistant, Mr. C. Watts, for his advice.

The financial assistance from my supervisor Dr. R. F. Frindt through a research grant from the Natural Sciences and Engineering Reasearch Council of Canada along with

the teaching assistantships from the Physics Department of S. F. U. are also very gratefully acknowledged.

Finally, I would like to thank Rich, without whose constant encourgement and support, without whose patiance in repeated proof reading, the thesis would not look as it does now.

Table of Contents

Approval ii

Abstract iii

Acknowledgments iv

List of Tables viii

List of Figures ix

Chapter 1. Introduction 1

1.1. MoS_2 1

1.2. Intercalation of MoS_2 3

1.3. Exfoliation of MoS_2 4

1.4. Restacking MoS_2 with foreign species included 5

1.5. The contribution of the thesis 7

Chapter 2. X-Ray Diffraction Method for an Assembly of Crystallites 8

2.1. Bragg's Law. Ewald construction for three-dimensional crystals 8

2.2. Ewald construction for two-dimensional systems 12

2.3. Powder method 14

2.4. Reflection from oriented films 18

2.5. Transmission from oriented films 19

2.6. Review of X-ray powder diffraction for single layer MoS_2 system 23

Chapter 3. Preparing the TCE Inclusion System of Restacked MoS_2 26

Chapter 4. Using X-Ray Diffraction Methods to Study the Structure of MoS_2/TCE and Restacked MoS_2 30

4.1. X-ray reflection of MoS_2/TCE and Restacked MoS_2 films 30

4.1.1. Sample preparation 30

4.1.2. X-ray results and discussion 30
4.1.3. TCE concentration in MoS_2/TCE by weight measurement 33
4.2. X-ray transmission of MoS_2/TCE and Restacked MoS_2 films 34
4.2.1. Sample preparation 34
4.2.2. Results and discussion 36
4.3. X-ray reflection on MoS_2/TCE and Restacked MoS_2 "powder" samples 38
4.3.1. Sample preparation 38
4.3.2. Results and discussion 38
4.4. Calculating the electron density distribution from the X-ray reflection pattern of the MoS_2/TCE oriented film 40
4.5. Calculating the MoS_2 basal plane orientation distribution of the Restacked MoS_2 film using the rocking curve experiments 44
Chapter 5. Optical Absorption and Electrical Resistance Measurements 50
5.1. Optical absorption spectra of MoS_2/TCE and Restacked MoS_2 films 51
5.2. Resistance versus temperature measurement of MoS_2/TCE and Restacked MoS_2 films 53
Chapter 6. Conclusions 57
Appendix. X-ray Transmission Patterns for MoS_2/H_2O and Restacked MoS_2 films 59
Bibliography 62

List of Tables

Table		Page
4.1	Intramolecular parameters of tetrachloroethylene (TCE)	32
4.2	List of (00l) line intensities and structure factors of MoS_2/TCE	43
6.1	Summary of structure parameters and physical properties of MoS_2/TCE and Restacked MoS_2 in comparison with 2H-MoS_2 crystal	58

List of Figures

Figure		Page
1.1	The layered structure of MoS_2	1
1.2	Coordination units for MoS_2	2
1.3	The structures of the MoS_2 polytypes	3
1.4	The structure of the organic inclusion MoS_2 system	6
2.1	Diffraction of X-rays by a crystal lattice	9
2.2	Scattering vector	10
2.3	Construction of Ewald sphere	11
2.4	The comparison of the Bravais lattice and reciprocal lattice for three-dimensional and two-dimensional periodic structures	12
2.5	Ewald construction for a two-dimensional system	13
2.6	Powder diffraction represented in the reciprocal space	14
2.7	Schematic drawing of a Philips diffractometer	15
2.8	Powder diffraction for two-dimensional systems represented in reciprocal lattice space	15
2.9	A comparison of X-ray diffraction patterns of three-dimensional, two-dimensional and one-dimensional powders	17

2.10 X-ray reflection from an oriented film 18

2.11 Reciprocal space representation of the reflection from an oriented film 18

2.12 X-ray transmission through an oriented film 19

2.13 Reciprocal space representation of the X-ray transmission through an oriented film 19

2.14 The schematic drawing of the Siemens D5000 Θ/Θ Diffractometer 20

2.15 The design of the sample changer on the Siemens D5000 Θ/Θ Diffractometer 21

2.16 The design of the sample holder for X-ray an transmission experiment 22

2.17 The sample holder in the sample changer 23

2.18 X-ray reflection patterns of MoS_2 powder 25

3.1 The preparation of single-molecular-layer MoS_2 27

3.2 Spreading MoS_2 film 29

4.1 The X-ray reflection patterns for oriented films 31

4.2 The structure of tetrachloroethylene (TCE) 32

4.3 A schematic drawing to show how nine MoS_2 molecules accommodate one TCE molecule 34

4.4 Transfer the MoS_2/TCE film to a Kapton substrate 35

4.5	X-ray transmission patterns for oriented films	36
4.6	X-ray reflection patterns for "powder" samples	39
4.7	X-ray reflection patterns of an MoS_2/TCE oriented film	42
4.8	The relative electron density distribution along the **c** direction of an MoS_2/TCE film	43
4.9	X-rocking curve measurement	44
4.10	The rocking curve of the 2H-MoS_2 random oriented powder	45
4.11	A geometric effect accompanying the rocking curve measurements is caused by the focus function of the diffractometer	46
4.12	The rocking curve of the Restacked MoS_2 film	47
4.13	The orientation distribution of the MoS_2 basal planes in the Restacked MoS_2 film on glass substrate	48
5.1	Comparison of d-band density of states of 1T-MoS_2 and 2H-MoS_2 based on Mattheiss's calculation	50
5.2	Room temperature optical absorption spectra of O#1 (MoS_2/TCE film) and O#2 (Restacked MoS_2 film)	52
5.3	Four probe variable temperature electrical conductivity data for a polycrystalline pellet of $(PEO)_{0.92}MoS_2$	53
5.4	(a) The sample geometry for the four probe resistance measurement; (b) The equivalent circuit	54

5.5 Resistance versus temperature data for MoS_2/TCE film using four probe geometry 55

5.6 Resistance versus temperature data for (a) MoS_2/TCE film; and (b) a film with a mixed phase of MoS_2/TCE and Restacked MoS_2 56

A.1 X-ray transmission patterns for MoS_2/H_2O and Restacked MoS_2 oriented films 60

Chapter 1
Introduction

1.1. MoS_2

Molybdenum disulfide, MoS_2, is a member of the transition metal dichalcogenide family. It is used as a catalyst in the petroleum industry and is also widely used as a lubricant. Its highly anisotropic structure and properties attract a great deal of interest.

MoS_2 has a layered structure consisting of MoS_2 sandwiches held together by a relatively weak interaction usually referred to as the Van der Waals force (Fig.1.1). Each MoS_2 sandwich layer is composed of one molybdenum sheet in between two sheets of sulfur. The atoms in a sheet form a two-dimensional triangular net. The separation between the Mo sheet and the S sheet is 1.59Å. The distance between the Mo sheets of adjacent sandwich layers is 6.15Å.

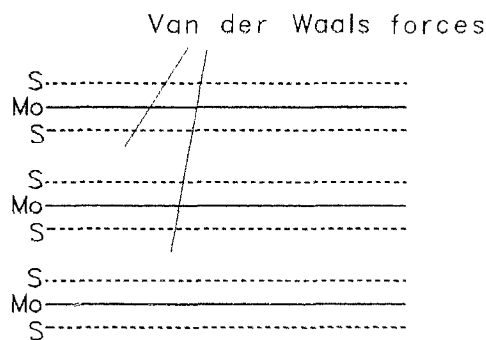

Fig.1.1 The layered structure of MoS_2

The force which bonds the MoS_2 sandwich layers together is relatively weak in comparison with the intra-layer bonding between Mo atoms and S atoms. This introduces very anisotropic physical properties for the material. MoS_2 crystals cleave at the Van der

Waals gaps between sulfur sheets. A sample as thin as a few molecular layers thick can be made using mechanical methods[1]. Because of the weak interlayer bonding, foreign materials can be inserted into the Van der Waals gap and under appropriate conditions the layers can be further separated to form single molecular layers.

Another interesting fact about MoS_2 is that there are two possible Mo coordinations when it is bonded with sulfur atoms. The Mo atom can be in a trigonal prismatic site (Fig.1.2 (a)) or in an octahedral site (Fig. 1.2 (b)). The different coordination of the Mo atom leads to different energy band structures which are crucial to the electrical and optical properties of the material.

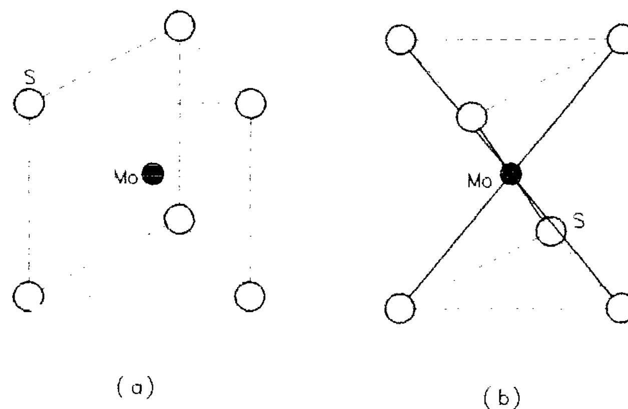

Fig.1.2 Coordination units for MoS_2
(a) trigonal prism (b) octahedron

So far as we know, crystalline MoS_2 has three polytypes: 1T, 2H and 3R (Fig.1.3). The integer indicates the number of layers per unit cell and T, H, R denote the trigonal, hexagonal and rhombohedral primitive unit cells respectively. The 2H and 3R stacking polytypes are found in naturally grown crystals. In both of the 2H and 3R polytypes, Mo atoms are at the trigonal prism site. The 1T polytype is new synthetic material[2] in which the Mo atom is at a slightly distorted octahedral site with a $\sqrt{3}a_0 \times \sqrt{3}a_0$ superlattice structure.

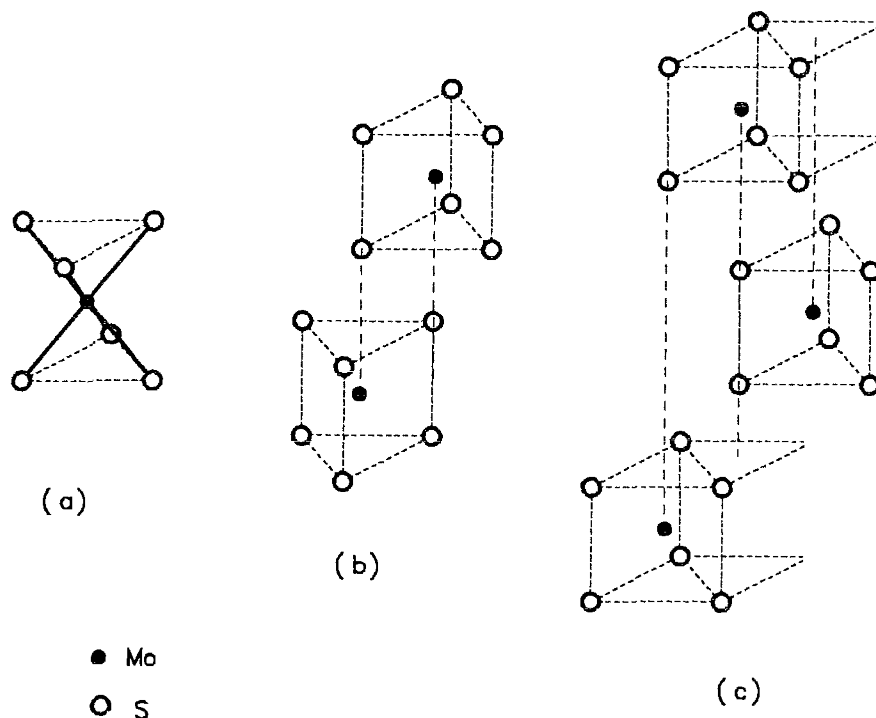

Fig. 1.3 The structures of the MoS_2 polytypes
(a) 1T MoS_2 /AbC/ (b) 2H MoS_2 /AbA BaB/ (c) 3R MoS_2 /AbA BcB CaC/

1.2. Intercalation of MoS_2

Intercalation refers to insertion of foreign species into the host structure. It is generally accepted that the tendency of charge to transfer from guest molecules or atoms, i.e., intercalants, to the host MoS_2 is the driving force for intercalation. A variety of electron-donating species ranging from Lewis bases to the low ionization energy metals have been intercalated into transition metal dichalcogenides with layered structures.

As for MoS_2, the weak bonding between the sulfur across the Van der Waals gap provides the possibility of introducing foreign atoms or molecules between the layers. Various alkali metals or ions can be inserted into MoS_2. The intercalation can drastically change the structure of the MoS_2 and its electronic properties. For example, a

semiconductor to metal transition has been observed optically during the intercalation of 2H-MoS_2 with sodium[3]. When 2H-MoS_2 is intercalated with lithium, the coordination of the Mo atom undergoes a transition from trigonal prism to octahedron[4] accompanied by a 6% expansion of Mo-Mo distances along the basal plane. It has been reported recently that the 2H to 1T structure change upon intercalation is also accompanied by a $2a_0 \times 2a_0$ superstructure[5]. An explanation for this structural transition is that when electrons are donated by the guest atoms or ions, the octahedral coordination can bring the system to a lower energy level[4].

1.3. Exfoliation of MoS_2

A process in which single molecular layers are formed is called exfoliation. It is an important process since it yields "two-dimensional" systems which are interesting from both a theoretical and experimental point of view.

The exfoliation of MoS_2 is the first example of exfoliating semiconducting layered compounds[6]. The process starts from Lithium intercalated MoS_2, i. e., Li_xMoS_2 (where x $\approx$ 1). The Li_xMoS_2 is then reacted with water. The reaction produces LiOH (Soluble) and hydrogen gas which "blows" the MoS_2 layers apart. Exfoliated MoS_2 in water suspension is in the form of one molecular thick sheets of MoS_2 usually referred to as "single-layer MoS_2".

It is reported that the Mo atom in single-layer MoS_2 also has the octahedral coordination, the same as in the lithium intercalated MoS_2. In addition, a strong lattice distortion is also observed for single layer MoS_2 through X-ray diffraction studies[7] and scanning tunneling microscopy[8].

1.4. Restacking MoS_2 with foreign species included

Foreign atoms or molecules can be inserted between the layers of the host structure by intercalation. However, the variety of material which can be used as intercalant is still quite limited. For example, no report yet shows that organic molecules can be inserted between MoS_2 layers by intercalation. Exfoliation opens a new route for building the so-called nanocomposites, in which different components are organized at the molecular scale. The single layers obtained through exfoliation are brought into full contact with the guest materials desired to be included and as the layers are allowed to stack up the guest atoms are thus trapped between the layers inside the resulting structure.

One technique for restacking MoS_2 with organic material is the spreading film method[9]. In this method, a single-layer MoS_2 water suspension of appropriate concentration and a water-immiscible organic liquid are introduced into the same container. After the mixture is shaken together in the container, the MoS_2 single layers leave the water and collect at the water-organic interface. Also, the collected layers will spontaneously spread up the walls of a glass container. If a wetted glass slide, rod or tube is dipped in, the collected layers will spread along the surfaces. Thus, a thin uniform film can be formed on the glass substrate. The film is found to be highly oriented with the basal plane of MoS_2 layers aligned parallel to the surface of the substrate.

A range of organic materials, such as benzene, styrene, tetrachloroethylene, etc., have been inserted between MoS_2 layers using the spreading film method. Some solid materials at room temperature, for example, ferrocene, can also be included by first being dissolved in an organic solvent and then applying the spreading film method. The basic structure of the resulting film is the same, namely a stack of parallel MoS_2 sheets with one or two molecular layers of guest molecules between MoS_2 layers (Fig. 1.4). The distance between the MoS_2 layers thus can range from 6.2Å (the interlayer distance for the MoS_2

crystal) to as big as 56.8Å (for MoS_2-stearamide) depending on the molecular size of the inserted species.

Besides the spreading film method, there are other ways to construct layer type complexes from single-layer MoS_2. Recently, some organic polymers, such as polyaniline, poly-ethylene-oxide, etc., have been encapsulated into MoS_2[10]. The addition of these polymer solutions to the single-layer MoS_2 water suspension causes flocculation during which the polymer chains are bound between the MoS_2 layers. The flocculation method has also been used to include metal atoms between MoS_2 layers[11] utilizing the fact the MoS_2 single layers tend to restack in a low pH environment.

There is rising interest in the organic inclusion compounds of MoS_2 since such organic/inorganic combinations have some potential for a wide range characteristics which come from both organic and inorganic components. There has been much work done on the structure study of the new composites. However, most of the work that has been done concerns the interlayer spacing of the host MoS_2 because such studies provide straightforward information about whether or not the attempt of including the guest species was successful. The study of MoS_2 basal plane coordination structure has not yet been reported although the Mo coordination plays an important role in the electronic and optical performance of the composites.

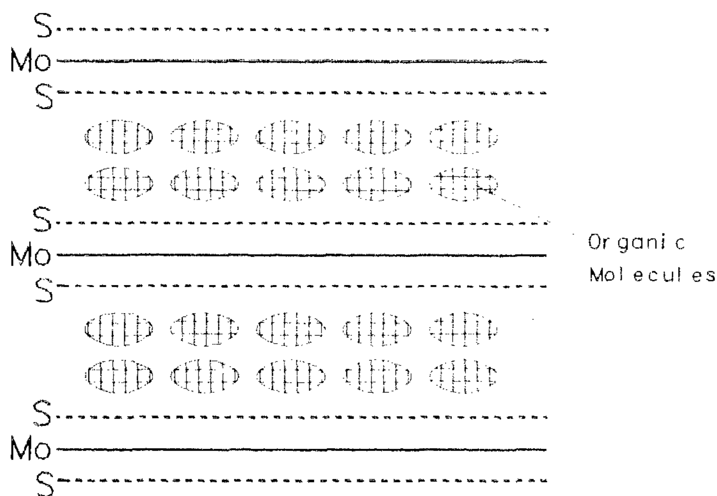

Fig. 1.4. The structure of organic inclusion MoS_2 system

1.5. The contribution of the thesis

In this project, we studied MoS_2 with an organic material — Tetrachloroethylene (TCE) included between the layers. TCE is chosen since it is a water immiscible organic liquid for which the spreading film technique is readily applicable. Also, TCE is transparent. This makes it easier to investigate the optical properties of the MoS_2 component. Moreover, the planar shape of the TCE molecule is useful in determining the molecular orientation.

The intent throughout the whole study was to elucidate the relation between the MoS_2 basal plane structure and the presence of the organic material. For this purpose, two systems were studied:

- ***MoS_2/TCE***—an inclusion system of organic tetrachloroethylene (TCE) molecules in restacked single molecular layer MoS_2.
- ***Restacked MoS_2***—the remaining material after desorption of TCE from MoS_2/TCE by heating.

The content of the thesis is arranged according to the techniques used. Chapter 2 introduces the X-ray diffraction techniques used in the structure study and also some important results obtained previously for the single-layer MoS_2 system which we will use to analyze our experimental result. A review of X-ray powder diffraction theory for two-dimensional systems is also included in Chapter 2. Chapter 3 describes making MoS_2/TCE systems using the spreading film method. All the X-ray diffraction studies of MoS_2/TCE and Restacked MoS_2 are reported in Chapter 4. Optical and electrical measurements are described in Chapter 5 and Chapter 6 gives a brief conclusion of the work.

Chapter 2
X-Ray Diffraction Methods for an Assembly of Crystallites

In this chapter, we intend to accomplish three main tasks. The first is to review the X-ray diffraction methods which we used in our structure study of the MoS_2/TCE system. The Ewald construction will be used throughout the whole introduction of the X-ray diffraction theory. Hopefully this approach will provide a basic understanding of the X-ray diffraction patterns obtained from the experiments without involving detailed calculation. The second task to be accomplished is to introduce the apparatus used in our experiments. The Philips Diffractometer and The Siemens D5000 Θ/Θ Diffractometer will be described only briefly since they are conventional instruments for structure study. However, the sample holder for X-ray transmission measurement will be explained in more detail, because it was designed particularly for our project. Finally, we are going to review some important results concerning X-ray powder diffraction for the single-layer MoS_2 system.

2.1. Bragg's Law. Ewald construction for three-dimensional Crystals

Since the typical inter-atomic distances in a solid are on the order of an angstrom and common X-rays have a wavelength of 1Å to 2Å, X-ray diffraction emerges as a powerful method for investigating the periodic structure of crystalline materials.

The structure of all crystals can be described in terms of a lattice[12]. The lattice is defined by three fundamental translation vectors $\mathbf{a}_1$, $\mathbf{a}_2$, $\mathbf{a}_3$ such that the atomic

arrangement looks the same in every respect when viewed from the point **r** as when viewed from the point

$$\mathbf{r}' = \mathbf{r} + u_1\mathbf{a}_1 + u_2\mathbf{a}_2 + u_3\mathbf{a}_3 \tag{2.1}$$

where u_1, u_2, u_3 are arbitrary integers. The set of points $\mathbf{r}'$ defined by (2.1) for all u_1, u_2, u_3 defines a lattice. A lattice is a regular periodic array of points in space. The lattice point represents a group of atoms, a structural unit. Therefore a lattice represents a crystal structure which is a repetition of single structural unit. When the structural unit is chosen to be the smallest possible, $\mathbf{a}_1$, $\mathbf{a}_2$ and $\mathbf{a}_3$ are called the primitive vectors, and the corresponding lattice is called the Bravais lattice.

The X-ray diffraction method is based on the constructive interference of X-rays. In Fig.2.1, a section of a crystal is shown. We can imagine that the lattice points are arranged on a set of parallel planes called lattice planes. When the incident X-rays strike the lattice points with an angle θ to the planes, they will be scattered in all directions. However, if we look at the lattice points on the same plane, for example point A and point B, only when the scattered beams make the same angle θ with the lattice plane, as shown in the figure, will the path lengths between the wavefronts shown be equal for different lattice points. Under such conditions they are in phase and constructively interfere. Rays which strike lattice points on adjacent planes have a different length of path. If the distance between the two lattice planes is d', the difference of path length is 2d'sinθ. Therefore the condition for them to be in phase and constructively interfere is that this difference of path length be equal to a whole number n of

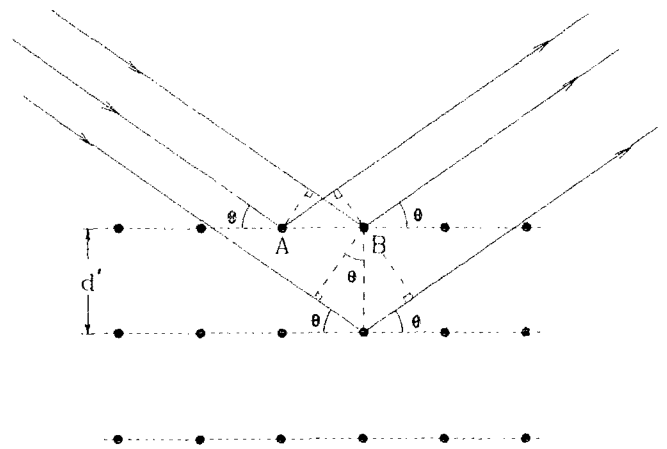

Fig.2.1 Diffraction of X-rays by a crystal lattice

X-ray wavelengths, λ, i.e.,

$$n\lambda = 2d'\sin\theta. \tag{2.2}$$

For convenience, we set $d = d'/n$ and the equation can be rewritten as

$$\lambda = 2d\sin\theta. \tag{2.3}$$

Equation (2.2) and (2.3) are both called the Bragg equation.

The phenomenon by which a large number of scattered rays can mutually reinforce each other is called diffraction. The Bragg equation states the essential condition which must be met if diffraction is to occur.

A lattice plane is defined to be any plane containing at least three non-collinear Bravais lattice points. Each set of lattice planes is a group of parallel planes with equal distance between them. A vector $\mathbf{K}_{hkl}$ is introduced to describe the set of lattice planes. With the chosen primitive vectors $\mathbf{a}_1$, $\mathbf{a}_2$, $\mathbf{a}_3$, the reciprocal lattice can be generated by using the basis vectors:

$$\mathbf{b}_1 = \frac{\mathbf{a}_2 \times \mathbf{a}_3}{\mathbf{a}_1 \cdot (\mathbf{a}_2 \times \mathbf{a}_3)}, \quad \mathbf{b}_2 = \frac{\mathbf{a}_3 \times \mathbf{a}_1}{\mathbf{a}_1 \cdot (\mathbf{a}_2 \times \mathbf{a}_3)}, \quad \mathbf{b}_3 = \frac{\mathbf{a}_1 \times \mathbf{a}_2}{\mathbf{a}_1 \cdot (\mathbf{a}_2 \times \mathbf{a}_3)} \tag{2.4}$$

and $\mathbf{K}_{hkl} = h\mathbf{b}_1+k\mathbf{b}_2+l\mathbf{b}_3$. The magnitude of the vector $\mathbf{K}_{hkl}$ is the reciprocal of the interplane distance d, i.e., $|\mathbf{K}_{hkl}| = 1/d$. $\mathbf{K}_{hkl}$ is perpendicular to the set of lattice planes which it is describing. The components of $\mathbf{K}_{hkl}$ in reciprocal space, h, k, l, can be used to index the lattice planes. The beam diffracted by the set of planes will be called the (hkl) beam and the peak related to this beam in the X-ray diffraction pattern will be labeled the (hkl) peak or the (hkl) line, etc.

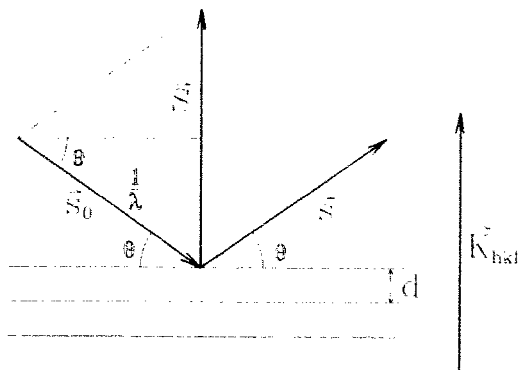

Fig.2.2 Scattering vector

If $\mathbf{s}_0$ and $\mathbf{s}$ are vectors in the direction of the incident beam and the diffracted beam respectively, each with magnitude of $1/\lambda$, then the vector $\mathbf{S} = \mathbf{s} - \mathbf{s}_0$ is called the scattering vector.

In terms of $\mathbf{K}_{hkl}$ and scattering vector $\mathbf{S}$, the Bragg law can be rewritten as:

$$\mathbf{K}_{hkl} = \mathbf{S} \tag{2.5}$$

The fact that $\mathbf{K}_{hkl}$ is along the same direction as $\mathbf{S}$ means that the scattering vector $\mathbf{S}$ is perpendicular to the set of lattice planes which "reflect" the X-ray beam and that the incident angle θ is just half of the total angle by which the incident beam is deflected. The fact that the magnitude of $\mathbf{K}_{hkl}$ is equal to $\mathbf{S}$ means:

$$|\mathbf{S}| = 2(1/\lambda)\text{Sin}\theta = |\mathbf{K}_{hkl}| = 1/d, \tag{2.6}$$

$$\text{i.e. } \lambda = 2d\text{Sin}\theta.$$

This is just the Bragg equation (2.3).

The Bragg law can be illustrated by the construction of the Ewald sphere. The reciprocal lattice is represented schematically by the dots in Fig.2.3. $\mathbf{s}_0$ is drawn along the direction of the incident X-ray beam and terminates at the origin of the reciprocal lattice.

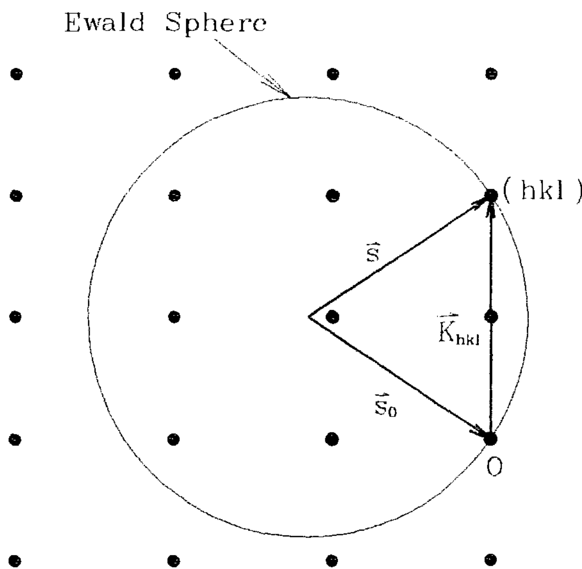

Fig.2.3 Construction of Ewald sphere

A sphere of radius $1/\lambda$ is centered at the initial end of $\mathbf{s}_0$ and passes through the origin, since the length of $\mathbf{s}_0$ is $1/\lambda$. The sphere is called the Ewald sphere or the sphere of reflection. Any reciprocal lattice point (h, k, l) which happens to fall on the surface of the Ewald sphere corresponds to the reciprocal vector $\mathbf{K}_{hkl}$ which represents a set of planes (hkl) for which the Bragg law is satisfied. $\mathbf{s}$ starts from

the center of the sphere and terminates at the point hkl, so the scattering vector $\mathbf{S} = \mathbf{s} - \mathbf{s}_0 = \mathbf{K}_{hkl}$. The angle between **s** and $\mathbf{s}_0$ is 2θ, twice the Bragg angle.

2.2. Ewald construction for two-dimensional systems

A one-dimensional system may be defined as a structure which only has periodicity in one direction. Similarly, a two-dimensional system may be defined as a structure which has periodicity in two directions only. A linear chain is an example of a one-dimensional system and a single layer of MoS_2 is a good example of a two-dimensional system.

The Ewald construction can be done for a two-dimensional system. First, we shall look at the reciprocal lattice for the two-dimensional systems. Fig. 2.4 demonstrates, with a tetragonal lattice as an example, how a three-dimensional system degenerates to a two-dimensional system.

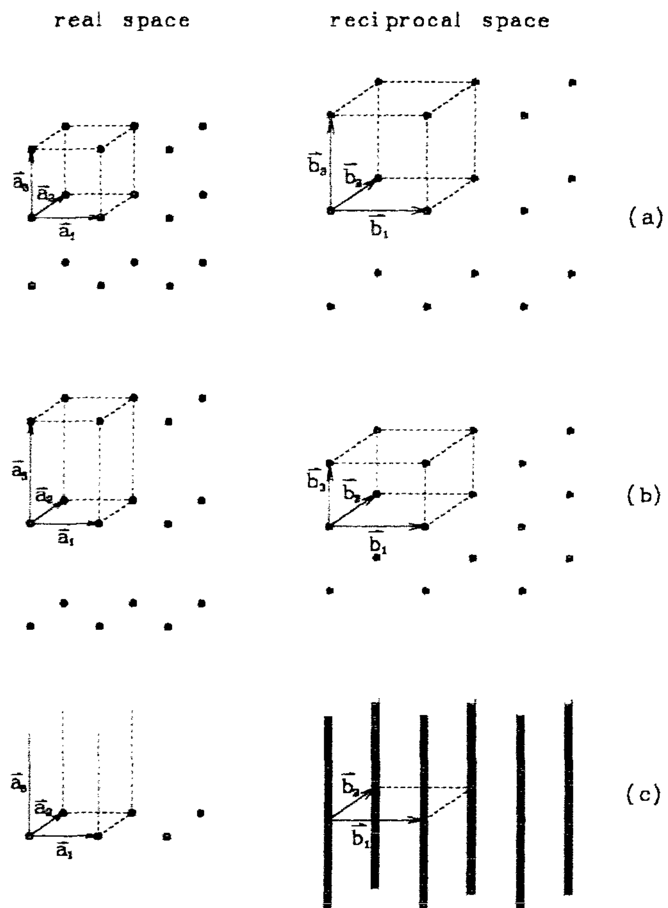

Fig.2.4 The comparison of the Bravais lattice and reciprocal lattice for three-dimensional and two-dimensional periodic structures

Fig.2.4(a) shows a simple cubic lattice with $a_1 = a_2 = a_3 = a$. The corresponding reciprocal lattice is also a simple cubic and $b_1 = b_2 = b_3 = 1/a$. In Fig.2.4 (b), the lattice vector is stretched, so $a_3 > a_1 = a_2$. This change shows in the reciprocal lattice with $b_3 < b_1 = b_2$.

Fig.2.4 (c) is the extreme case of Fig.2.4 (b) for $a_3 \rightarrow \infty$. This is a lattice with periodicity in only two directions, i. e., a two-dimensional lattice. The corresponding reciprocal lattice will become a lattice with $b_3 \rightarrow 0$. That is, the reciprocal lattice becomes a series of lines parallel to each other. For finite sized 2-dimensional layers, the reciprocal lattice is a series of parallel "rods" rather than lines. The smaller size the crystal is, i.e., the fewer unit cell each single crystal contains, the thicker the reciprocal rods become.

The construction of the Ewald sphere starts from the reciprocal lattice of the two-dimensional system (Fig.2.5). $\mathbf{s}_0$ is along the direction of the incident X-ray beam and terminates at the origin O on the reciprocal rod (00). The Ewald sphere which has the radius $1/\lambda$ is centered at the initial end of $\mathbf{s}_0$ and passes through the origin O. Bragg's law is satisfied at all positions where the Ewald sphere intersects a reciprocal rod.

There are (hk0) lines but no (hkl) (h or k $\neq$ 0 and l $\neq$ 0) or (00l) lines in the diffraction pattern for a two-dimensional system since there is no periodicity along the $\mathbf{a}_3$ direction.

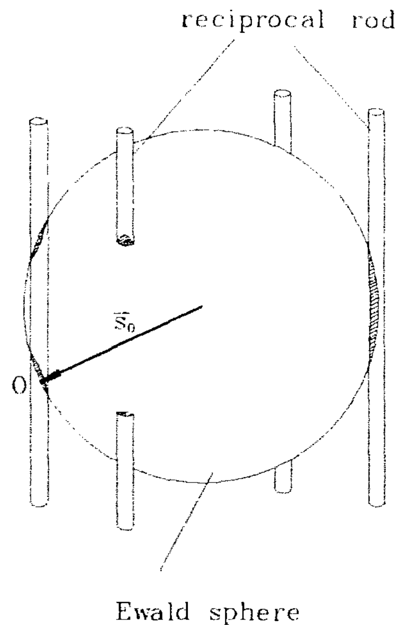

Fig.2.5 Ewald construction for a two-dimensional system

2.3. Powder method

In the powder method, the crystal to be examined is reduced to a very fine powder and placed in a beam of monochromatic X-rays. Each particle of the powder is a tiny crystal, or assemblage of smaller crystals, oriented at random with respect to the incident beam. This random orientation of the crystal powder corresponds to the random rotation of the reciprocal lattice around its origin. For any given diffracted beam direction, $\mathbf{S} = \mathbf{s} - \mathbf{s}_0$ is given. We may consider the reciprocal lattice to be fixed and let $\mathbf{S}$ rotate randomly around the origin of the reciprocal lattice. The tip of the vector $\mathbf{S}$ traces out a spherical surface $\mathcal{S}$ (Fig.2.6). Since the tip of the vector $\mathbf{S}$ is on the Ewald sphere, any reciprocal lattice point which falls on the surface $\mathcal{S}$ should satisfy the Bragg condition. That is, the intensity of the diffracted beam reaches its peak value at the given direction. As we can see here, the random orientation of the sample powder determines that the satisfaction of the Bragg condition only depends on the magnitude of the scattering vector $\mathbf{S}$, i. e., the radius of sphere $\mathcal{S}$. Therefore, any reciprocal lattice point associated with a scattering vector $\mathbf{S}$ of magnitude within the measurement range should appear as a peak referred to as (hkl) line in the diffraction pattern.

In this project, the Philips diffractometer equipped with a Type 150 100 00 Wide Range Goniometer using nickel-filtered Cu K_α radiation was used for X-ray powder diffraction measurement. The main features of the Philips diffractometer are shown in Fig.2.7. A is the monochromatic incident X-ray beam coming from the source X-ray tube T. The sample is mounted on the sample

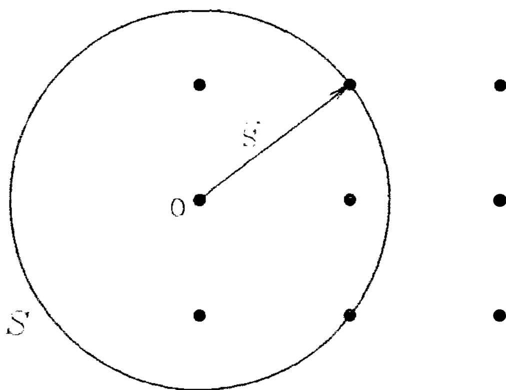

Fig.2.6 Powder diffraction represented in the reciprocal space

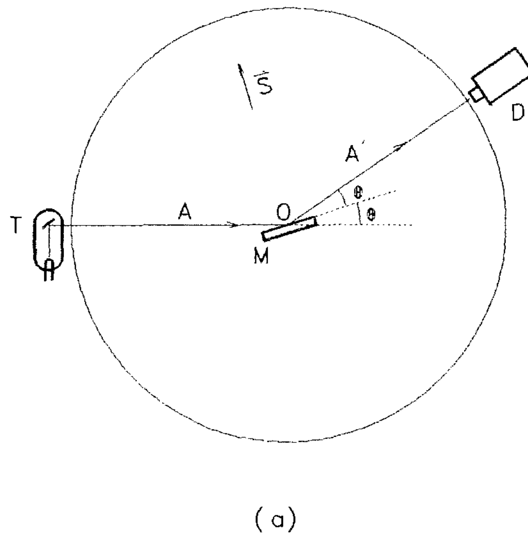

Fig. 2.7 Schematic drawing of a Philips diffractometer

holder M which can rotate around the axis O perpendicular to the paper. D is an X-ray detector which can move along the circle centered at O. Generally, OD rotates twice as fast as the sample holder M so that the angle between beam A and the holder is equal to the angle between beam A′, which is detected by the detector D, and the sample holder. This angle θ changes when the detector and the sample holder rotate around O. When the Bragg condition is satisfied, the detector receives a high intensity X-ray signal. This is shown as a peak in the X-ray pattern which shows the relation between the angle θ and X-ray intensity. From the peak position, i.e. the value of θ, we can calculate the lattice plane spacing of the sample by using the Bragg equation (2.1).

The X-ray diffraction intensity versus 2θ pattern for three-dimensional crystal powder appears as a series of sharp peaks. However, if the powder is of random oriented two-dimensional crystallites, the situation changes, as we see from the Ewald construction (Fig.2.8). The reciprocal lattice for two-dimensional systems is a set of parallel rods. A sphere S with radius 2Sinθ/λ is

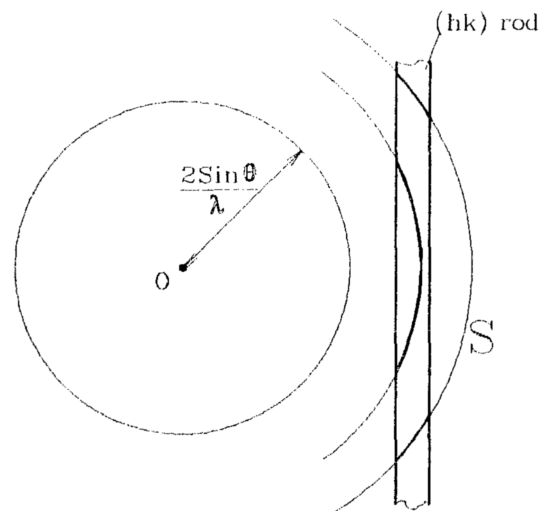

Fig.2.8 Powder diffraction for two-dimensional systems represented in reciprocal lattice space

centered at the origin of the reciprocal lattice. This sphere S corresponds to some θ. The X-ray intensity at the given θ depends on the intersection of the sphere S and the reciprocal rod, say, (hk) rod. When θ is increasing, the sphere is expanding. After the sphere touches the rod, the X-ray intensity starts to increase. When the sphere expands to a certain point beyond the center of the rod, the intersection between the sphere S and the (hk) rod reaches its maximum and the X-ray intensity reaches its maximum value. The sphere S continues to expand and the intersection becomes smaller but never reaches zero since the reciprocal rods extend infinitely. The X-ray powder diffraction pattern for two-dimensional system appears as a peak which sharply increases on low angle side and slowly decreases on the high angle side. The peak shape largely depends on the scattering factors since they determine the "intensity" distribution of the reciprocal rod.

An extensive study of the X-ray powder diffraction pattern for two-dimensional MoS_2 (single-layer MoS_2 system) has been completed by Datong Yang, et al. Fig.2.9 is extracted from the Ph.D. thesis of D. Yang. It is a comparison of X-ray powder diffraction patterns of three-dimensional and two-dimensional MoS_2 systems. Both curves are obtained by direct computer calculation using the Debye formula assuming that the Mo coordination is trigonal prism.

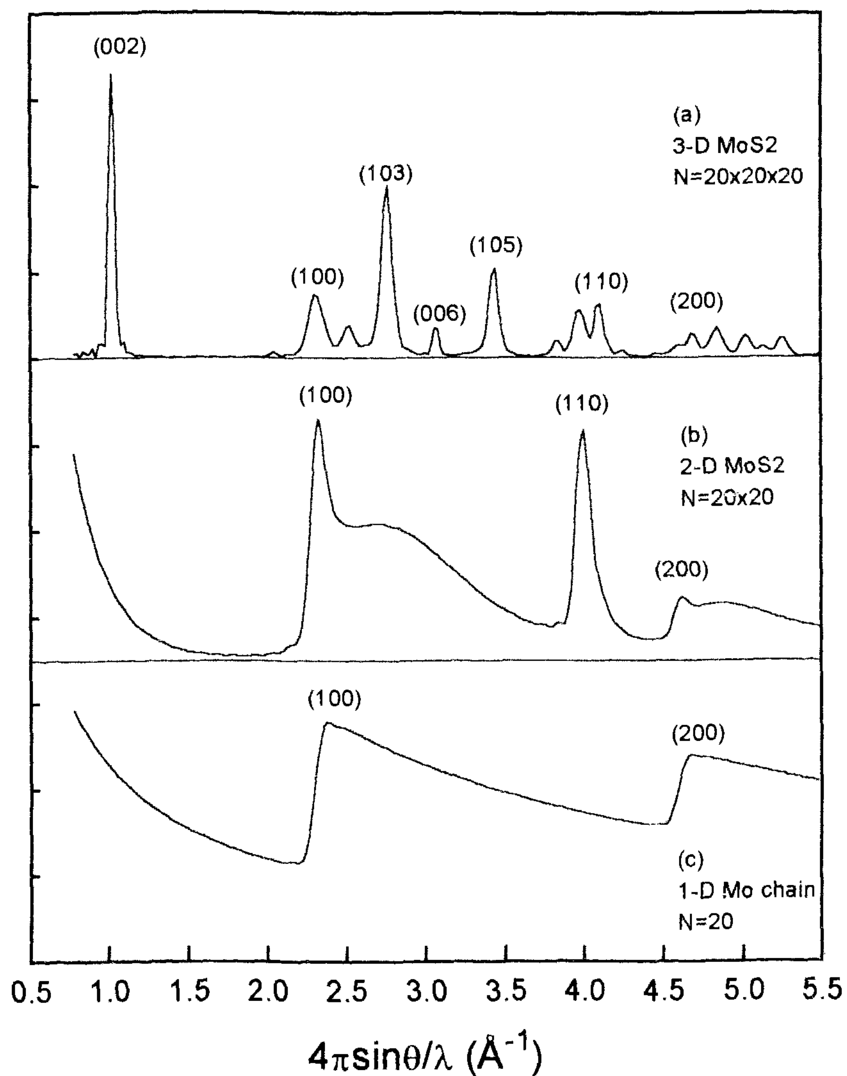

Fig. 2.9 (Fig. 1.1 of the Ph.D. thesis of Datong Yang, 1993)
A comparison of X-ray diffraction patterns of three-dimensional, two-dimensional and one-dimensional powders. (a) A three-dimensional 2H-crystal; crystal size: 20×20×20 unit cells. (b) a two-dimensional single layer; layer size: 20×20 unit cells. (c) A one dimensional linear array of 20 atoms. All curves were obtained by direct computer calculation using the Debye formula.

2.4. Reflection from oriented films

An "oriented" film is an assembly of two-dimensional crystallites in which all basal planes are parallel to each other. For an oriented film, X-ray reflection refers to a measurement setting in which both the incident beam and the diffracted beam are on the same side of the film and the X-ray scattering vector **S** is perpendicular to the film, as shown in Fig.2.10. Fig 2.8., which was developed for a two-dimensional random powder, should be modified to meet the new condition. The condition that the crystallites can only rotate on the substrate surface provides a restriction, in that the scattering vector **S** must always be perpendicular to the basal planes of these crystallites and therefore parallel to the correspondent reciprocal rod (hk). Under such restriction, the sphere S degenerates to only two points on the (00) rod (Fig.2.11). These are the only places at which Bragg conditions can be satisfied. Therefore, there are no (hkl) lines shown in the X-ray diffraction pattern. However, if the basal planes are evenly spaced, the X-ray pattern will have sharp (00l) peaks which reflect the spacing d between the basal planes.

The Philips diffractometer was used for X-ray reflection of oriented MoS_2 films in

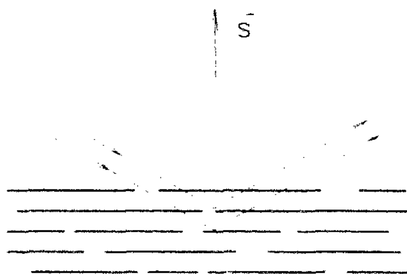

Fig. 2.10 X-ray reflection from an oriented film.
The scattering vector S is perpendicular to the basal planes

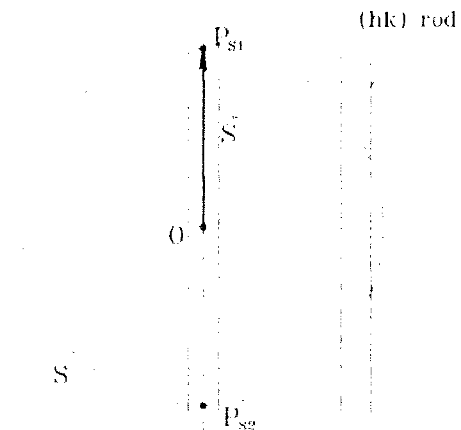

Fig. 2.11 Reciprocal space representation of the reflection from an oriented film.
In reciprocal space, sphere S is degenerated into two points, P_{s1} and P_{s2}, on the axis of the reciprocal rod (00)

this project.

2.5. Transmission from oriented films

Reflection patterns from MoS_2 oriented films do not carry any information about the structure within the basal planes. In order to study the basal plane structure, the orientation of the films with respect to the X-ray beams has to be changed. The measurement setting for transmission from oriented films is such that the incident beam and the diffracted beam are on different sides of the sample film, and the scattering vector **S** is along the film. Also, as shown in Fig.2.12, the incident beam and the diffracted beam are on a plane perpendicular to the film. Fig 2.13 shows the Ewald construction for the transmission from oriented film. Since the scattering vector **S** is always on a plane parallel to the film, i.e., parallel to the basal planes of the crystallites, it is perpendicular to the correspondent reciprocal rods. The sphere S which corresponds to random oriented crystallites now reduces to a circle C_S. At a given θ or **S** value, the X-ray intensity for the (hk0) peak depends on the intersection of C_S and the (hk) rod. When increasing θ (increasing $|\mathbf{S}|$), the area of intersection follows a sudden increasing—reaching the

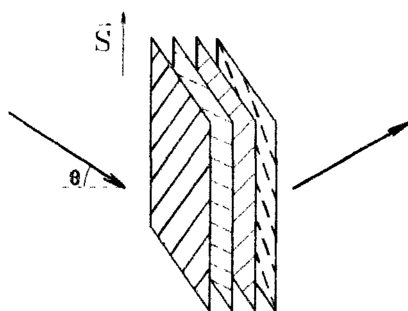

Fig.2.12 X-ray transmission through an oriented film. X-ray beams are on a plane perpendicular to the film

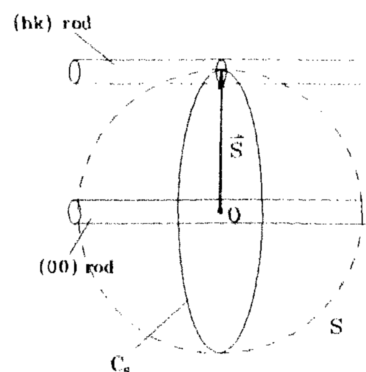

Fig.2.13 Reciprocal space representation of the X-ray transmission through an oriented film. The sphere S is degenerated into a circle perpendicular to the reciprocal rods

maximum—sudden decreasing manner. This is similar to the three-dimensional case. The X-ray pattern should thus show a series of sharp (hk0) peaks.

The X-ray transmission pattern from an oriented film carries information about the basal plane structure which is absent in the reflection pattern. This method was used to investigate the MoS_2 basal plane structure of oriented MoS_2/TCE films and Restacked MoS_2 film.

The Siemens D5000 Θ/Θ Diffractometer was used to perform the X-ray transmission experiments in our project. The design of the diffractometer is schematically shown in Fig. 2.14. The diffractometer is generally used for diffraction measurement of a powder sample with a flat surface. The sample changer of the diffractometer can hold the sample horizontally, and the measurement circle is centered at point O on the surface of the sample.

The focus of the X-ray tube T, sample H and the detector diaphragm D are on the focusing circle. The focus of the tube and the detector are also located on the measuring circle. They can rotate independently around the center of the measure circle O. A is an aperture diaphragm which is set between the X-ray tube and sample which delimits the irradiated sample area. The aperture diaphragm rotates around O together with the tube. S is the scattered radiation diaphragm which is used to suppress the undesired scattered radiation. It is aligned with the detector diaphragm D and the detector.

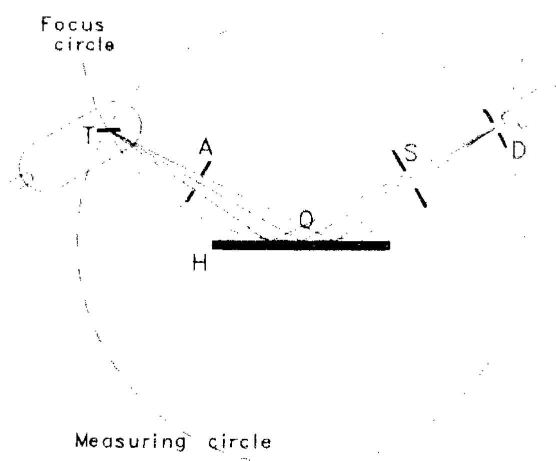

Fig.2.14 The schematic drawing of the Siemens D5000 Θ/Θ Diffractometer

Fig. 2.15 shows the basic features of the sample changer where (a) is the front view of the sample changer and (b) is the top view. SS are three stop screws. The tips of these stop screws define the horizontal plane in which the center of the measuring circle O is traced. P is the pressure unit which can hold the sample H tightly against the stop screws so that the sample surface passes through the center of the measure circle and is on a line tangential to the focus circle. There is a 2.7 cm wide gap between the two arms A1 and A2 holding the stop screws. This provides a path for the X-rays. Incidentally, it also makes it possible for us to insert a vertical sample in the gap for the transmission measurement.

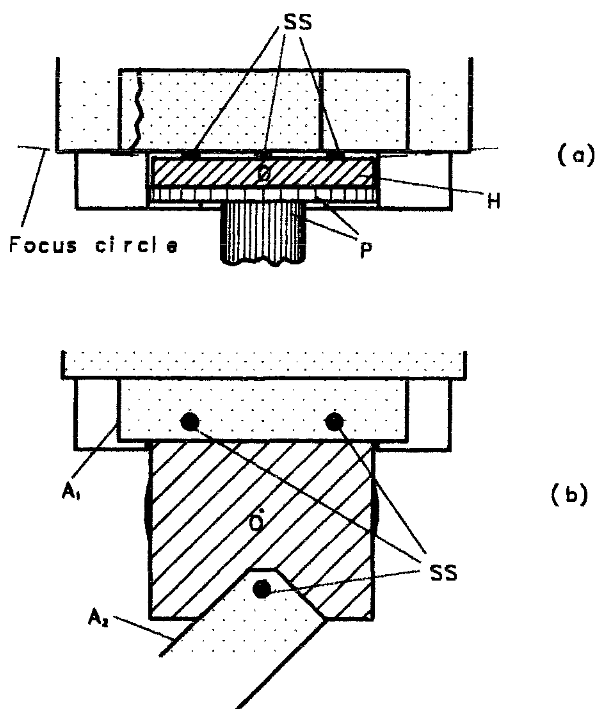

Fig.2.15 The design of the sample changer on the Siemens D5000 Θ/Θ Diffractometer
(a) front view (b) top view
(proportional drawing)

Since the Siemens Diffractometer is designed to perform reflection measurements from a flat sample surface, in order to use it to perform X-ray transmission, it was necessary to present a vertical film which would be "transparent" or thin enough to allow the X-rays to pass through it and be received by the detector on the other side of the film. To achieve this, the sample film was deposited on a thin Kapton (a trade name of a fluorinated polyamide thin film) substrate and a specialized holder was designed to hold the substrate vertically in the machine.

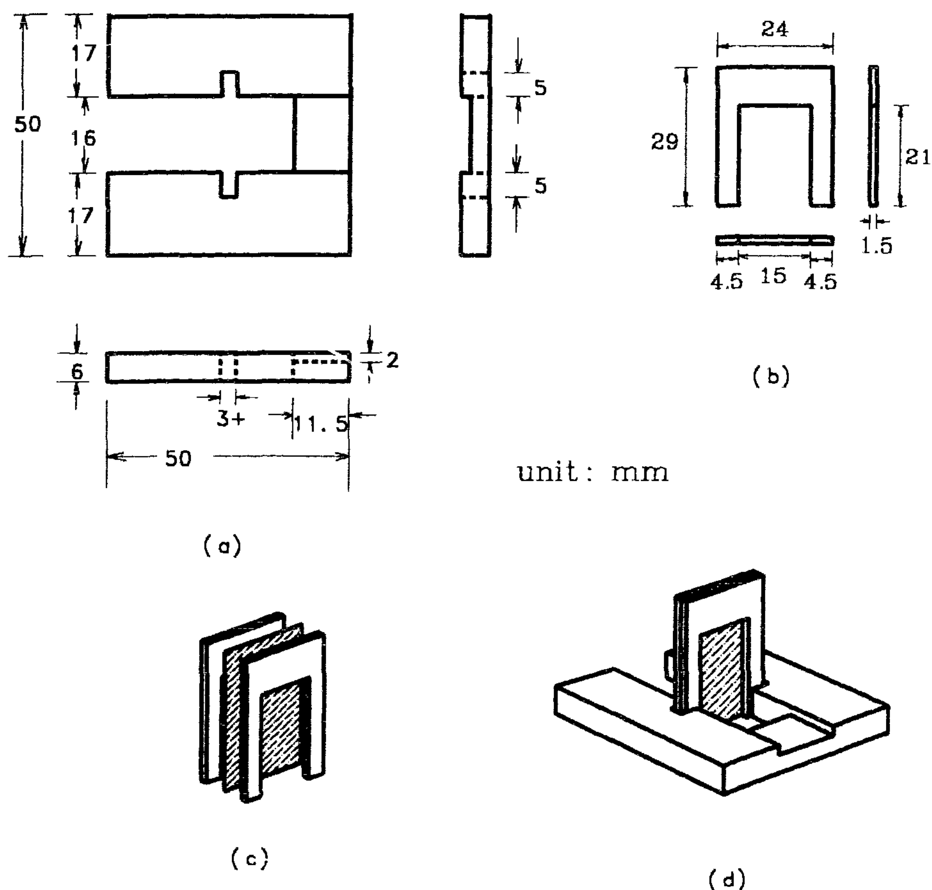

Fig.2.16 The design of the sample holder for an X-ray transmission experiment

Fig.2.16 shows the design of the sample holder. The base of the sample holder was made by cutting a piece of aluminum plate (50mm×50mm×6mm) into a "U" shape(Fig.2.16(a)). There is one notch on each arm of the "U" to hold the Kapton clamp. The Kapton clamp is a combination of two identical smaller "U" shaped aluminum pieces(Fig.2.16(b)). The clamp holding the sample film on Kapton substrate is inserted into the notches in the base and is kept perpendicular to the base as shown in Fig.2.16(c)&(d). Thus the geometry provides a Kapton substrate of size 20mm×15mm.

The sample holder fits in the sample changer of the diffractometer. Fig.2.17(a) shows the top view of the fitting and Fig.2.17(b) shows the intersection along LL' line.

For the diffraction measurement, 1° slits have been chosen for the aperture diaphragm A and the scattered radiation diaphragm S. A 0.6mm slit is chosen for the detector diaphragm D which delimits the area of sample studied to a range from 16mm× 0.5mm to 16mm×0.8mm varying depending on the θ value. The Siemens D5000 diffractometer uses Cu Kα radiation, with a wavelength of 1.542Å.

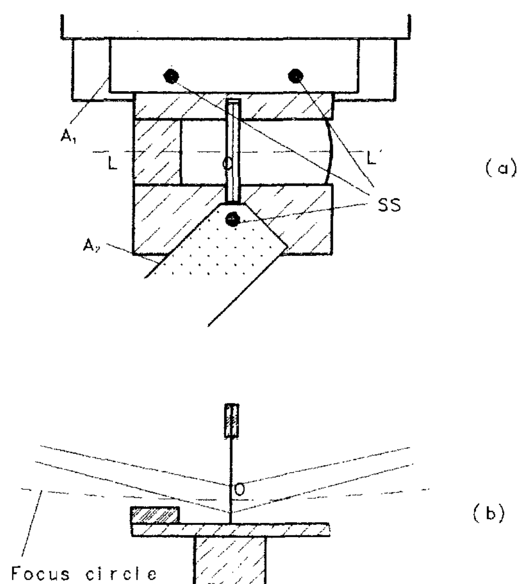

Fig.2.17 The sample holder in the sample changer

2.6. Review of X-ray powder diffraction for single layer MoS_2 system

Fig.2.18 is extracted from the Ph.D. thesis of Datong Yang. This single figure serves our need well and the details are contained in the explanation accompanying the figure. Here we will add a few extra words about the systems involved in the figure.

(a), (b) and (c) are all about single layer MoS_2 systems which are assemblies of single molecular layer MoS_2 flakes. These flakes are oriented in random directions. These systems are two-dimensional powder systems. (d) shows data for a three-dimensional powder sample in which the MoS_2 layers have orderly stacking, one on top of another. From (b) and (c), we may clearly see that the (200) line shape is closely related to the coordination of Mo in MoS_2 layers. When the Mo is at the octahedral site, the (200) line possesses a saw tooth shape. However, if Mo coordination is trigonal prismatic, the (200)

line is a combination of a sharp spike on the low angle side with a long tail on the high angle side. The comparison of experimental result (a) and the calculation (b) and (c) shows that in single layer MoS_2, Mo has an octahedral coordination. The labeling of the lines follows the conventional choice of MoS_2 unit cell. The angle between $\mathbf{a}_1$ and $\mathbf{a}_2$ is 120° and, for a non-distorted lattice, the magnitudes of $\mathbf{a}_1$ and $\mathbf{a}_2$ are both equal to the distance between two adjacent Mo atoms. $\mathbf{a}_3$ is chosen to be perpendicular to the MoS_2 layer for three-dimensional crystal. For a distorted lattice with the $2a_0 \times 2a_0$ superstructure, the magnitudes of $\mathbf{a}_1$ and $\mathbf{a}_2$ double and in the reciprocal space, the magnitude of $\mathbf{b}_1$ and $\mathbf{b}_2$ reduce to half of their original value. Therefore the (h k l) lattice planes for the non-distorted lattice correspond to the (2h 2k 2l) lattice planes for the distorted lattice with a $2a_0 \times 2a_0$ superstructure.

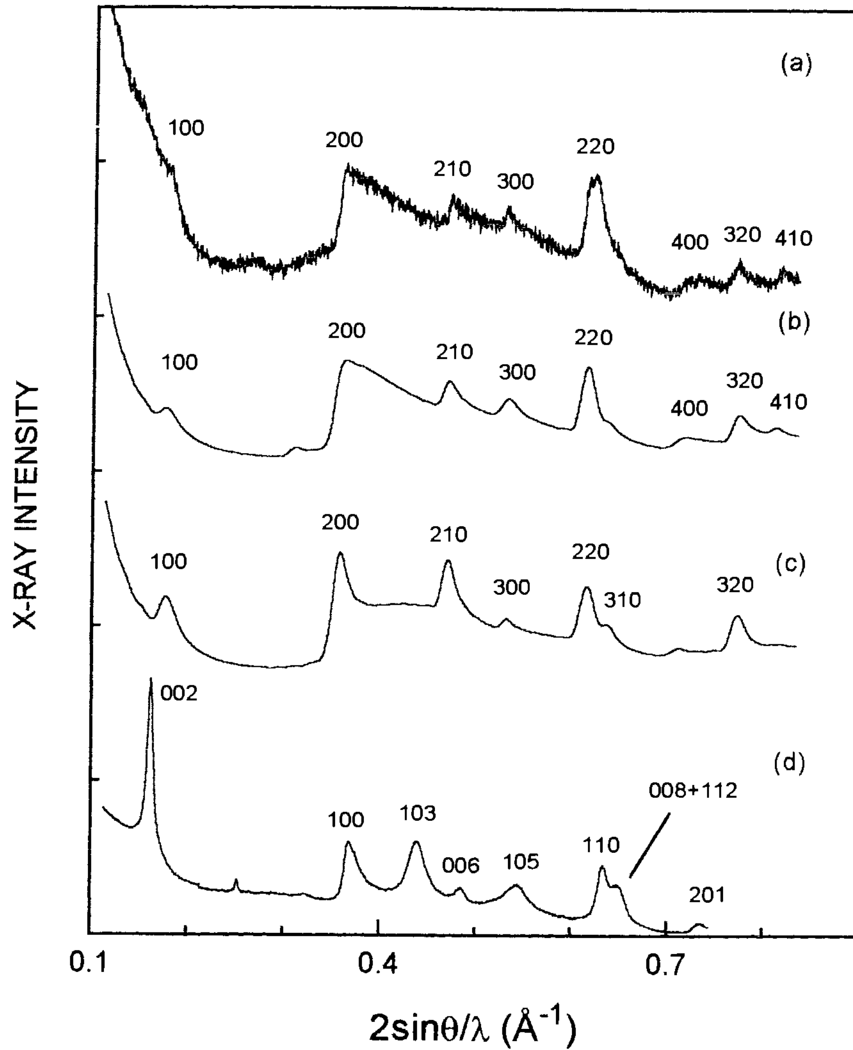

Fig.2.18 X-ray reflection patterns of MoS_2 powder
(Yang, Datong, Ph.D. Thesis, Figure 6.1)

(a) Experimental pattern of single layer MoS_2 suspended in water. The background due to water and substrate has been subtracted.

(b) Calculated pattern of distorted octahedral MoS_2 single layer. A $2a_0 \times 2a_0$ superstructure is introduced with a distortion of 0.14. The layer size is 20×20 units. An a_0=3.27Å was used.

(c) Calculated pattern of distorted trigonal prismatic MoS_2 single layer. All parameters are same as in (b).

(d) Experimental X-ray diffraction pattern of restacked, dried and baked MoS_2 sample. All (00l) lines and mixed lines of crystalline 2H-MoS_2 reappear and the a_0-spacing shifts back to 3.16Å.

Chapter 3
Preparing the TCE Inclusion System of Restacked MoS_2

The process of preparing the TCE (tetrachloroethylene) inclusion system of restacked MoS_2, i.e., the MoS_2/TCE system, may be divided into four steps: intercalation, exfoliation, forming a single-layer MoS_2 and organic mixture and making MoS_2/TCE films. Up to the exfoliation of MoS_2 to form single-layer MoS_2 water suspension, we followed the procedure which was first introduced by P. Joenson,et al[6] . To include TCE between restacked MoS_2 layers, we used the technique invented by W. M. R. Divigalpitiya, et al[9] . Now, we will explain how the process was performed step by step.

Step 1. Intercalation

One gram of 2H-MoS_2 powder (from Johnson Matthey Inc.) was weighed and put in a glass container. In an argon glove box, the MoS_2 powder was soaked in approximately 50 ml *2.5M n-butyl lithium solution in hexane* at room temperature for at least 48 hours (the container was tightly sealed). This process is know as intercalation (or lithiation). It results in lithium intercalated MoS_2, Li_xMoS_2, with $x \cong 1$. The sediment was then washed twice with hexane to remove the excess n-butyl lithium. After the sediment had settled, the liquid was decanted and the sediment was allowed to dry by evaporation of hexane. The vial containing lithiated MoS_2 was sealed and removed from the glove box.

Step 2. Exfoliation

The lithiated MoS_2 in the sealed vial was then placed under flowing distilled water and the cover was removed to let about 150ml of water in. A violent bubbling was observed. The container was then ultrasonicated for about 15 minutes and was shaken

occasionally during the ultrasonicating. Agitation helps the lithiated MoS_2 react with water to form hydrogen gas between MoS_2 layers. It is assumed that the expansion of this gas tends to help separate the layers of the crystal and allow water molecules to seep between the layers. A structure in which the MoS_2 layers are stacked turbostratically with two layers of water included between them is obtained up to this point[13]. The mixture was then centrifuged and decanted. The washing and centrifuging process was repeated three or four times to reduce the pH value, and a suspension of single-molecular-layer MoS_2 sheets in water was obtained.

The intercalation and exfoliation process is illustrated in Fig.3.1[13].

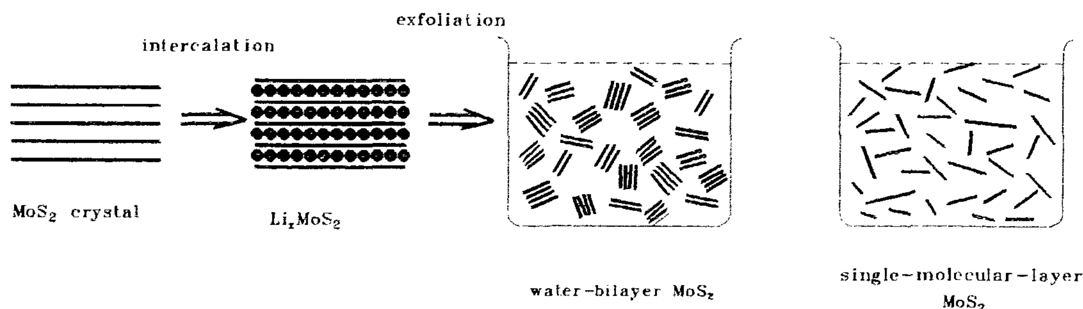

Fig.3.1 The preparation of single-molecular-layer MoS_2

Step 3. Forming single-layer MoS_2 and organic mixture

The single-molecular-layer MoS_2 water suspension was diluted with distilled water to approximately 3 mg/cc. Then, 10 ml to 15 ml of such suspension was introduced into a 90 ml wide-mouth vial (the glass wall of the vial was wetted by shaking the liquid inside). A suitable amount of Tetrachloroethylene liquid was carefully added into the container along the glass wall. The container was sealed. The mixture was then well circulated by

shaking or magnetic stirring in order to bring a good contact between MoS_2 layers and TCE molecules. After sufficient circulation, the suspension was allowed to settle and a stable interface to form between the more dense TCE and less dense water. Some dark gray clusters accumulated on the water/TCE interface and, meanwhile, a very uniform thin film of MoS_2/TCE could be observed climbing up along the glass wall of the container. (If the concentration of single-molecular-layer MoS_2 water suspension was as low as 1.5mg/cc and the volume of TCE added is equal to that of the single-molecular-layer MoS_2 water suspension, after circulation had ceased and the system had settled all the MoS_2 layers would gather at the water/TCE interface, the upper surface of the water phase and the glass wall of the container. The water appeared to be clear.) The system of the single-molecular-layer MoS_2 water suspension and liquid TCE at this stage is referred to as a "MoS_2-TCE two phase system".

Step 4. Making MoS_2/TCE film

MoS_2/TCE films used for measurement were obtained in two different ways. The first method is the so-called spreading film technique. Here a wet glass slide was dipped into the glass vial containing the MoS_2-TCE two phase system. The container was then sealed and shaken. When the liquid mixture settled, a uniform film spread up along the glass wall and the glass slide. In a couple of minutes, the glass slide was ready for withdrawal from the container. The film was allowed to dry naturally in the air. In this way, a uniform MoS_2/TCE film with 2.5 cm $\times$ 2.5 cm area was obtained. By repeating the same process, tens of such films could be made from the same MoS_2-TCE two phase system. A good shaking and long settling (overnight) is the key for successful film spreading at a later time. The process of forming the MoS_2-TCE two phase system and spreading film is shown in Fig.3.2. The MoS_2/TCE film obtained in this particular way will be referred to as a "spread film" throughout the latter part of the thesis.

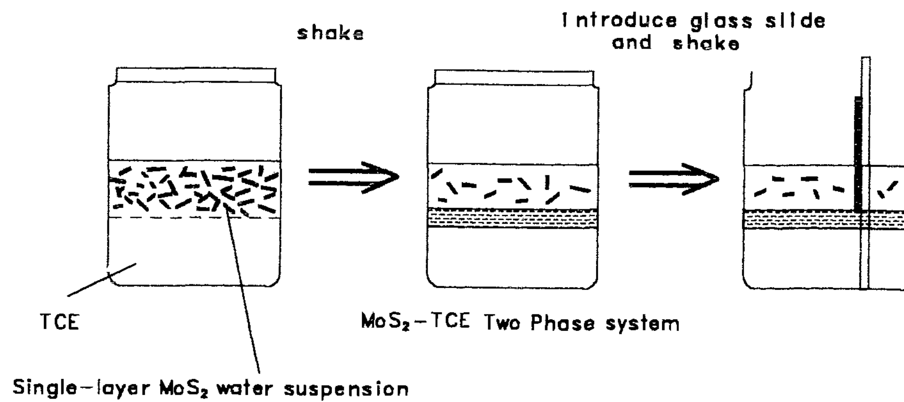

Fig.3.2 Spreading MoS_2 film

Another method used to make the MoS_2/TCE film was to draw some material from the interface of the MoS_2-TCE two phase system and then drop the material onto a flat substrate such as glass slide or sapphire plate. Drying of the material in air results in formation of a MoS_2/TCE film on the surface of the substrate. The MoS_2/TCE film obtained with this method will be referred to as "dropped film".

Chapter 4
Using X-Ray Diffraction Methods to Study the Structure of MoS_2/TCE and Restacked MoS_2

4.1. X-ray reflection of MoS_2/TCE and Restacked MoS_2 films

4.1.1. Sample preparation

Three systems have been studied using X-ray reflection. They are MoS_2/TCE, Restacked MoS_2 and a system with a mixed phase of MoS_2/TCE and Restacked MoS_2. The results for one sample of about ten from each kind of system are reported here. The samples are labeled as R#1, R#2 and R#3.

R#1 is a MoS_2/TCE spread film prepared using the method described in Chapter 3. The thickness of the film was measured using a polarization interferometer. It is between 300Å and 500Å. The film was deposited on a glass slide.

R#2 was obtained by heating a MoS_2/TCE spread film (same as R#1) at 250°C for 17 hours in a vacuum environment.

R#3 was obtained by heating a MoS_2/TCE spread film (same as R#1) at 100°C for 47 hours in a vacuum environment.

4.1.2. X-ray results and discussion

Fig.4.1 shows the X-ray reflection patterns for the three systems. For convenience in reading, the lines are off-set along the intensity axis.

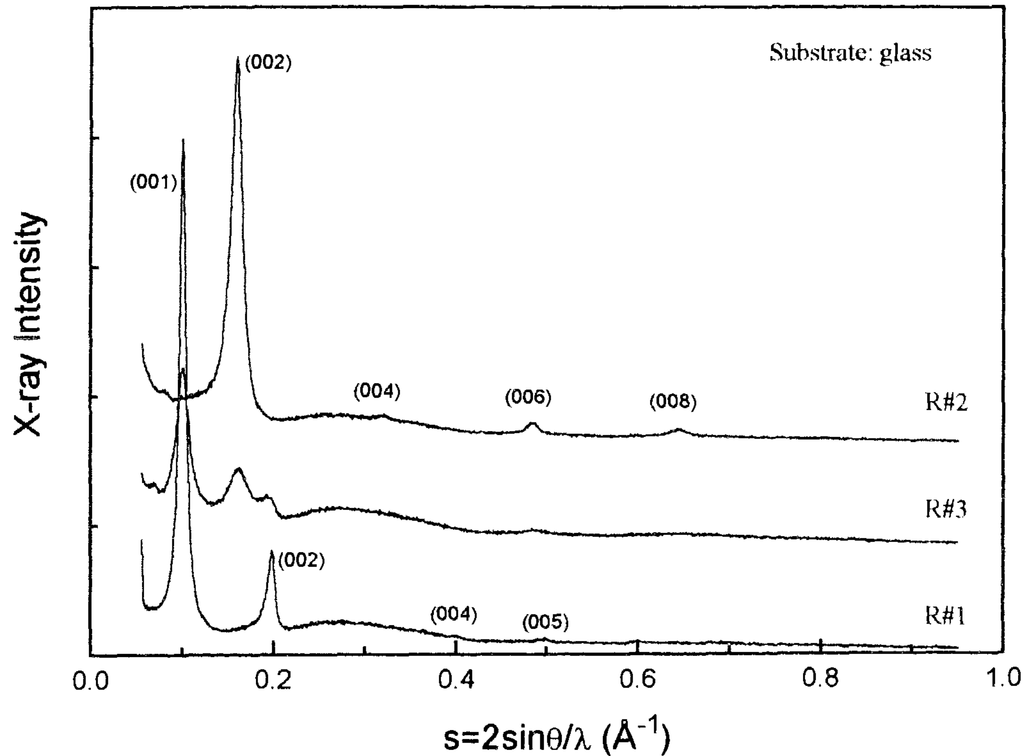

Fig.4.1 X-ray reflection patterns for oriented films

- Sample R#1: a MoS_2/TCE film
- Sample R#2: a Restacked MoS_2 film
- Sample R#3: a film with mixed phase of MoS_2/TCE and Restacked MoS_2

In all three curves, only (00l) lines appear. This indicates that all three systems are oriented films, with MoS_2 basal planes lying parallel to the surface of the glass substrate and therefore perpendicular to the scattering vector **S**.

For the MoS_2/TCE system (R#1), the positions of (001), (002), (004) and (005) correspond to an interlayer spacing of 10.02Å. This is a 60% expansion from the interlayer spacing of 6.17Å for the original 2H-MoS_2 crystals . To investigate what this

expansion means in relation to the molecular dimensions of TCE, a review of the molecular structure of TCE might be useful.

Table 4.1 Intramolecular parameters of tetrachloroethylene (TCE)

d (C-C)	1.310Å
d (C-Cl)	1.706Å
d (C Cl)	2.687Å
d (Cl...Cl),cis	2.901Å
d (Cl...Cl),cis	3.169Å
d (Cl...Cl),trans	4.294Å
∠ClCCl	112.35°
∠ClCC	125.47°

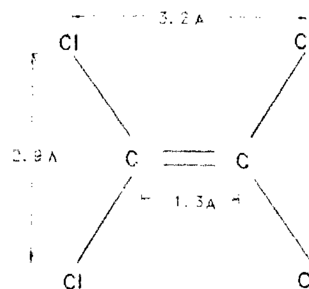

Fig.4.2 The structure of tetrachloroethylene (TCE)

Tetrachloroethylene (TCE) is a near planar molecule consisting of two carbon atoms and four chlorine atoms, as shown in Fig.4.2. The intramolecular parameters for liquid TCE are elucidated by neutron diffraction[14], and are listed in table 4.1. Assuming that the chlorine atom has the same radius as the chlorine ion (Cl^-) which is 1.81Å, we estimate the size of a TCE molecule to be 6.8Å×6.5Å×3.6Å.

The 3.85Å expansion of the interlayer spacing leaves enough room for one layer of TCE molecules to lie "flat" between MoS_2 layers.

For the Restacked MoS_2 system (R#2), the (001) peak position shows an interlayer spacing of 6.22Å. It is close to the value for the original MoS_2 crystal. This indicates a complete desorption of TCE from the system.

Curve R#3 shows a mixed phase in the process of transferring from MoS_2/TCE back to the Restacked MoS_2 structure. Two interlayer spacings co-exist in such a mixture. The intensities of the lines related to MoS_2/TCE decrease while the intensities of the lines related to the Restacked MoS_2 increase upon further desorption of TCE.

The X-ray reflection is easy to perform and it carries clear information about the sample status. We used it on a regular basis to distinguish between MoS_2/TCE and the Restacked MoS_2. However, for oriented films, the X-ray reflection does not provide any hint about the MoS_2 intralayer structure. This is when the X-ray transmission experiments come into play.

4.1.3. TCE concentration in MoS_2/TCE by weight measurement

The weight ratio of TCE to MoS_2/TCE was measured using an electronic balance. First, some MoS_2/TCE powder was examined using X-ray powder diffraction method and weighed, which was found to be 0.170 gram. The MoS_2/TCE powder was then baked in a vacuum oven at 250°C and weighed again. The weight of the baked material was 0.155 gram. Another X-ray diffraction measurement was followed to confirm that the baked material was Restacked MoS_2. The experimental data shows the weight percentage of TCE in MoS_2/TCE to be 8.8% assuming that there was no MoS_2 oxidized during heating.

The radio of the number of TCE molecules to the number of MoS_2 molecules in MoS_2/TCE can also be calculated:

$$\frac{N_{TCE}}{N_{MoS_2}} = \frac{M_{TCE} \,/\, m_{mol\,(TCE)}}{M_{MoS_2} \,/\, m_{mol\,(MoS_2)}} \approx 1{:}10.7, \tag{4.1}$$

where $\frac{M_{TCE}}{M_{MoS_2}} = \frac{0.015g}{0.170g - 0.015g}$, $m_{mol\,(TCE)} = 166g$ and $m_{mol\,(MoS_2)} = 160g$. Therefore, in the MoS_2/TCE system, about every eleven MoS_2 molecules can accommodate one TCE molecules.

Fig.4.3 provides us a rough idea about this situation by showing how nine molecules accommodate one TCE molecule along the MoS_2 basal plane. Obviously, there is no tight bonding between TCE molecules.

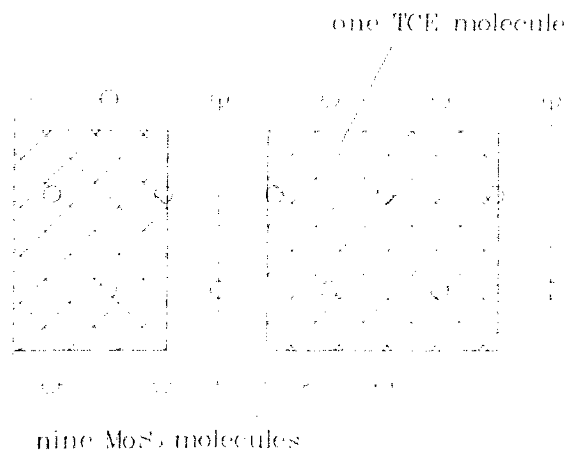

Fig.4.3 A schematic drawing to show how nine MoS_2 molecules accommodate one TCE molecule

4.2. X-ray transmission of MoS_2/TCE and Restacked MoS_2 films

4.2.1. Sample preparation

In X-ray transmission experiments, the X-ray beam reaching the detector has to penetrate through both the sample film and the substrate. The intensity of the beam is weakened by the absorption. To reach an optimum signal to noise ratio, we need to control two factors: the thickness of the sample film and the choice of a substrate. In general, the sample film should be thick enough to provide enough signal and both the sample and the substrate should not be too thick, otherwise a serious absorption would be introduced.

Kapton was chosen as the substrate. It is a rigid and thin film which can hold the MoS_2/TCE or Restacked MoS_2 film in a plane and allow a good X-ray penetration. It is also high temperature resistant which made the heat treatment of the sample more convenient. Kapton also has a low background in the diffraction patterns.

A spread film of MoS_2/TCE such as R#1 in the previous section is 300Å to 500Å thick. It is far too thin for an X-ray transmission experiment. To build a thicker sample film, we used the film transfer method which was first suggested by Divigalpitiya et al. The procedure is shown in Fig.4.4. The MoS_2/TCE spread film was released from the glass substrate onto the surface of distilled water by slowly immersing the glass slide in the water. Then, the film was picked up with a new substrate, the Kapton film. In this process, a piece of microscope cover glass was used to support the Kapton substrate. After the water on the film evaporated naturally, the procedure was repeated until a MoS_2/TCE film of desired thickness was obtained. The optimum thickness of the MoS_2/TCE film for the X-ray transmission measurement is around 1 micron.

The X-ray transmission pattern for two samples,T#1 and T#2, are presented here:

T#1 is a MoS_2/TCE film. The sample is made of a stack of 30 MoS_2/TCE spread films, making it around a micron thick.

T#2 is obtained by heating T#1 at 240°C for 5 hours in a vacuum environment. Heating helps extract the TCE molecules from the structure. The X-ray reflection experiment shows that T#2 is a Restacked MoS_2 system.

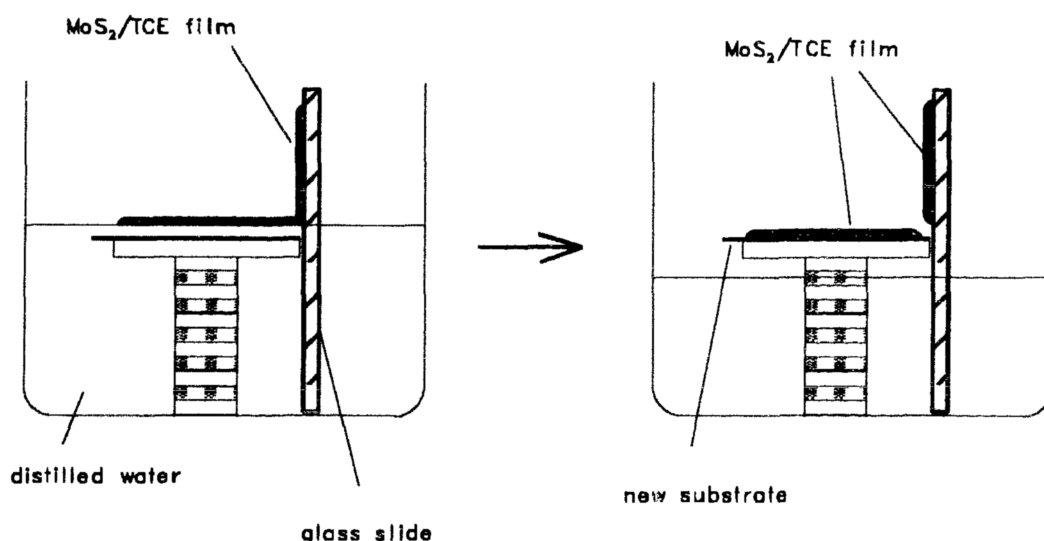

Fig.4.4 Transfer of the MoS_2/TCE films to a Kapton substrate

For a reference an X-ray transmission experiment was also performed for 2H-MoS_2 crystal powder held on a Kapton substrate with the same holder and under the same measurement condition as for the film samples.

4.2.2. Results and Discussion

The X-ray transmission patterns for sample T#1 and sample T#2 are shown in Fig 4.5. The two vertical lines mark the (100) and (110) peak positions for 2H-MoS_2 crystal powder. The background has been subtracted from the pattern.

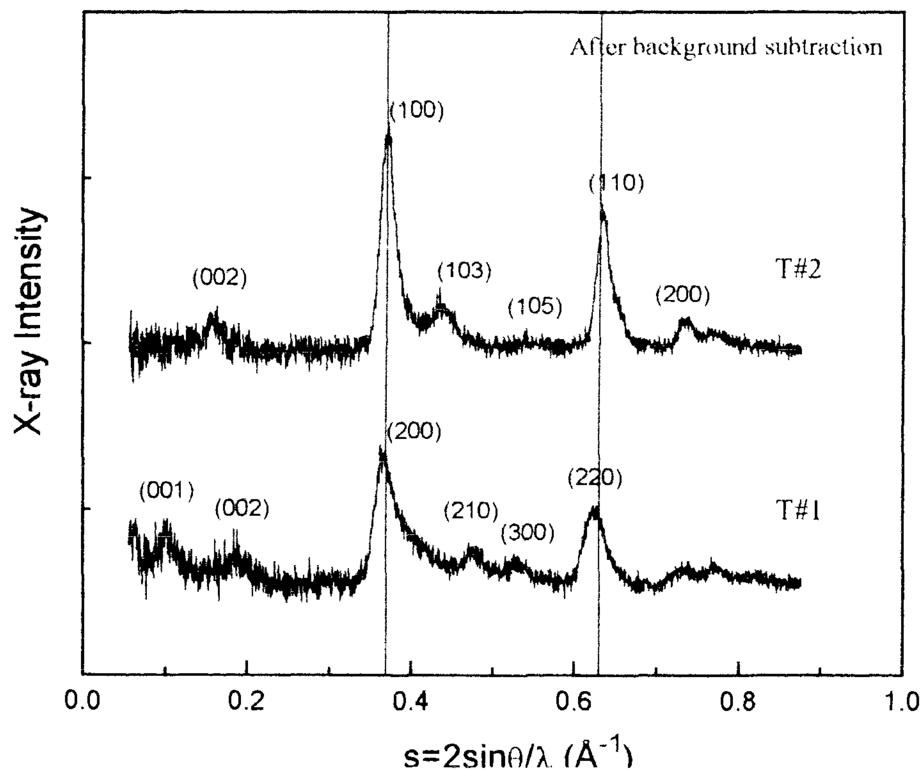

Fig.4.5 X-ray transmission patterns for oriented films

- Sample T#1: a MoS_2/TCE film
- Sample T#2: a Restacked MoS_2 film

From the pattern for T#1 (a MoS_2/TCE system), an expanded a-spacing and a superlattice structure are observed. The (200) peak and the (220) peak, which correspond to the (100) and (110) peaks for the 2H-MoS_2 crystal respectively, shift to the low angle side. From the (hk0) peak position, the a-spacing can be calculated. The average value obtained from (200), (210), (300) and (220) peak positions is 3.24Å. It is a 2.5% expansion from the original crystal a-spacing of 3.16Å. The (100), (210) and (300) peaks which appear in the X-ray transmission pattern for T#1 didn't appear in the X-ray powder diffraction pattern for 2H-MoS_2 crystal. They are superlattice peaks related to a $2a_0 \times 2a_0$ superlattice structure. This basal plane expansion accompanied with a lattice distortion is an important signature of the octahedrally coordinated MoS_2 which has been observed in Li-intercalated MoS_2[4,5] and single-layer MoS_2[7] . Therefore, from the X-ray transmission pattern for MoS_2/TCE, we may infer that the Mo atoms are in the octahedral coordination in MoS_2/TCE.

In the pattern for T#2 (a Restacked MoS_2 system), no superlattice peaks are observed. The (100) and (110) peaks are located at the same positions as the ones for the original 2H-MoS_2 powder with an a-spacing of 3.16Å. This indicates that the MoS_2 coordination has transferred back to the trigonal prism upon desorption of TCE from the structure.

As we have mentioned in section 2.5, the X-ray transmission pattern for a perfectly oriented film should only contain (hkO) peaks. Neither (001) peaks nor mixed (hkl) peaks should show up in the ideal case. However, in our X-ray transmission pattern for MoS_2/TCE and Restacked MoS_2 films, some (001) and (hkl) lines showed up as small peaks. This indicates that there was a small portion of material in our sample not oriented in the same direction as the majority of the sample.

4.3. X-ray reflection on MoS_2/TCE and Restacked MoS_2 "powder" samples

The purpose of performing X-ray diffraction on powder samples of both MoS_2/TCE and Restacked MoS_2 systems was to investigate whether the MoS_2 layers are turbostratically stacked or stacked with order between layers . The idea is that if the stacking is ordered, then the resulting system is a three-dimensional system and the mixed (hkl) lines should appear in the X-ray powder diffraction pattern.

4.3.1. Sample preparation

The results which are reported in the thesis are from two samples: P#1 and P#2. The preparation procedures were.

For P#1: Material deposited as MoS_2/TCE spread films was scraped off the glass slides. The collected material was then pressed onto the frosted end of a glass slide. This process may result in a powder sample with some degree of preferred orientation, although ideally a sample with perfect random oriented powder is desired.

P#2: Sample P#1 was heated at 250°C for 9 hours in a vacuum environment.

4.3.2. Results and discussion

The X-ray diffraction pattern for P#1 and P#2 are shown in Fig.4.6. The vertical lines mark the (100) and (110) peak positions for 2H-MoS_2 powder. The following conclusions can be drawn from the X-ray diffraction patterns:

1. The layers are turbostratically stacked within the MoS_2/TCE system. This is indicated by the fact that there are not any (hkl) mixed lines being observed in the X-ray diffraction pattern for sample P#1. In the X-ray pattern for Restacked MoS_2 powder (P#2), the mixed lines (103) and (105) appear. This means that there is some ordered

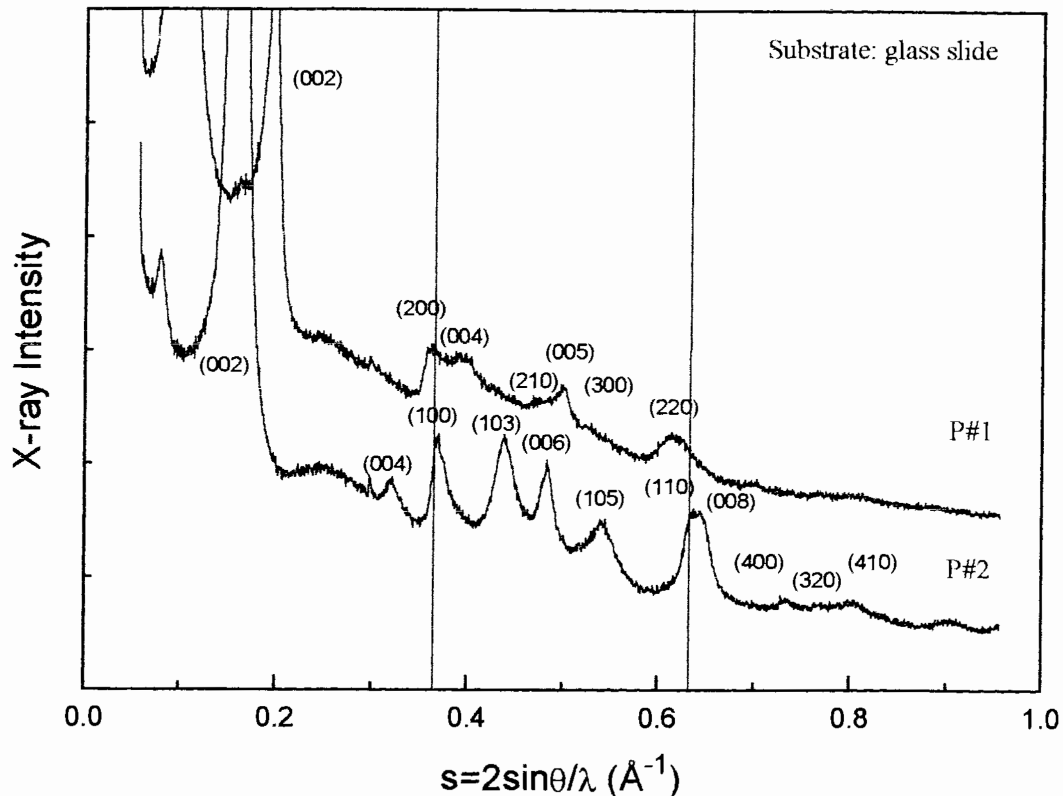

Fig.4.6 X-ray reflection patterns for "powder" samples

- Sample P#1: MoS_2/TCE powder
- Sample P#2: Restacked MoS_2 powder

stacking of layers upon desorption of TCE. The observed (100) to (103) line intensity ratio is about 1:1 which differs from that of the 2H- MoS_2 powder. This may due to a mixed 2H and 3R type stacking[15].

2. For MoS_2/TCE, the (200) and (220) peaks shift to low angle from the dotted lines which indicates an expanded a-spacing for MoS_2/TCE in comparison with that of the 2H-MoS_2 crystal. This expanded a-spacing is 3.25Å. It is calculated by averaging over the value obtained from (200), (210), (300) and (220) peak positions. The expanded a-spacing was also observed from X-ray transmission experiment. For the Restacked MoS_2, the data from P#2 shows that the a-spacing of 3.16Å for the 2H-MoS_2 crystal is restored.

3. For the MoS_2/TCE system, the (200) peak has a saw-tooth shape. This shows that Mo atoms are at the octahedral site in MoS_2/TCE.

The superlattice peaks we observed in X-ray transmission patterns for the MoS_2/TCE films are not obvious here. This is due to the present strong (005) peak which is positioned between the expected (210) and (300) superlattice peaks.

4.4. Calculating the electron density distribution from the X-ray reflection pattern of the MoS_2/TCE oriented film

The structure factor F_{hkl} is a concept frequently used in X-ray diffraction analysis. It is a quantity proportional to the X-ray scattering amplitude and thus directly related to the measured X-ray intensity.

The structure factor F_{hkl} is defined as an integral over a single unit cell:

$$F_{hkl} = \iiint_V \rho\,(x,y,z)\, e^{2\pi i(hx+ky+lz)}\, dv \qquad (4.2)$$

where V is over the volume of a unit cell, x, y, z are fractional coordinations and $\rho(x,y,z)$ is the electron density. From Equation (4.2), we can see that the structure factor F_{hkl} is actually a Fourier coefficient of $\rho(x,y,z)$[16,17], that is,

$$\rho\,(x,y,z) = \frac{1}{V}\sum_h \sum_k \sum_l F_{hkl}\, e^{-2\pi i(hx+ky+lz)} \qquad (4.3)$$

The electron density distribution along one direction:

$$\rho\,(z) = \frac{1}{L}\sum_{l=-\infty}^{+\infty} F_{00l}\, e^{-2\pi i lz} \qquad (4.4)$$

where L is the length of a unit cell along the considered direction.

For a centrosymmetric structure, $\rho\,(z) = \rho\,(-z)$. Therefore,

$$F_{00l} = \int_{-\frac{1}{2}}^{\frac{1}{2}} \rho\,(z)\, e^{-2\pi i lz}\, dz$$

$$= 2 \int_0^{\frac{1}{2}} \rho(z) \cos(2\pi l z)\, dz$$

is a real number. Moreover, if in the unit cell there is a heavy atom which possesses most of the electrons in the unit cell and which is located at $z = 0$, then the structure factor F_{00l} is also positive. Thus, from Equation (4.4),

$$\rho(z) = \frac{1}{L} |F_{000}| + \frac{2}{L} \sum_{l=1}^{+\infty} |F_{00l}| \cos(2\pi l z)$$

$$\text{i.e.} \quad \rho(z) = C + D \sum_{l=1}^{+\infty} |F_{00l}| \cos(2\pi l z) \qquad (4.5)$$

where C and D are constant.

The relation between the structure factor F_{hkl} and the X-ray intensity I_{hkl} of the (hkl) line at the Bragg angle θ is as follows[18],

$$I_{hkl} = K\, p\, |F_{hkl}|^2 \frac{1 + \cos^2(2\theta)}{\sin\theta \cos\theta} e^{-2M} \qquad (4.6)$$

where the multiplicity factor p is equal to 2 for all (00l) lines, $1+\cos^2(2\theta) = P(\theta)$ is the polarization factor and $(1/\sin\theta)(1/\cos\theta) = L(\theta)$ is the Lorentz factor. e^{-2M} is the temperature factor, where $M = B(\sin\theta/\lambda)^2$ and B is an adjustable parameter related to the magnitude of vibration. For an inorganic single crystal, B is normally between 2.5 and 3.5 and for an organic solid, B can be well beyond 10. The term K is a constant for any given set of measurements.

Equation (4.6) can be used to calculate the structure factor,

$$|F_{00l}| \propto |F'_{00l}| = \sqrt{\frac{\sin\theta \cos\theta}{1 + \cos^2(2\theta)} I_{00l} e^{2M}} \;,$$

where F'_{00l} is a relative structure factor. Directly following Equation (4.5), we get,

$$\rho(z) - C \propto \rho'(z) = \sum_{l=1}^{+\infty} |F'_{00l}| \cos(2\pi l z) \qquad (4.7)$$

where $\rho'(z)$ is a relative electron density distribution.

To calculate the electron density distribution along the **c** direction of MoS_2/TCE system, each Mo sheet, S sheet or TCE layer may be treated as a dot on a linear chain

along the **c** direction. This system is assumed centrosymmetric and Mo is the heavy atom in the unit cell, so Equation (4.7) is applicable.

Fig.4.7 is the X-ray diffraction pattern of the MoS_2/TCE oriented film. I_{00l} can be obtained by measuring the area under each intensity peak. Table 4.2 lists the measured I_{00l} values, θ values and the calculated $|F'_{00l}|$ values for B=0 and B=7. We have determined the relative electron density distribution ρ'(z) using equation (4.7) for any chosen z value with the approximation of taking only the first 8 terms of the sum using the peaks observed in Fig.4.7. The relative electron density ρ' versus z in a single unit cell along the **c** direction is shown in Fig.4.8.

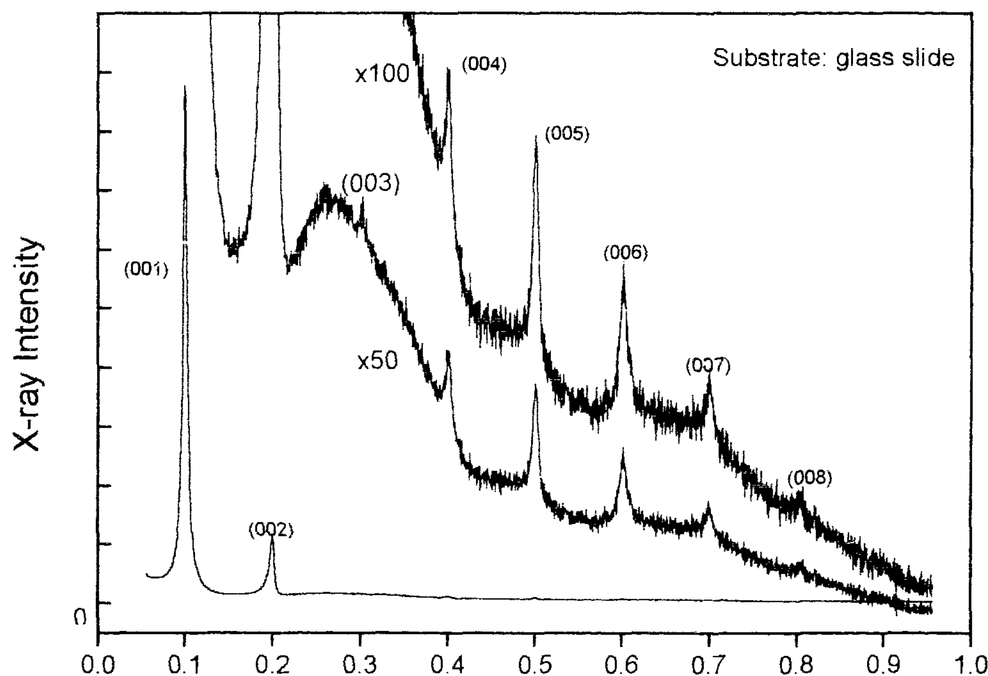

Fig.4.7 X-ray reflection patterns of an MoS_2/TCE oriented film

Table 4.2 List of (00l) line intensities and structure factors of MoS_2/TCE

l	θ	I_{00l}	$\|F'_{00l}\|$ (B=0)	$\|F'_{00l}\|$ (B=7)
1	4.43°	193.5	2.75	2.79
2	8.88°	21.5	1.31	1.40
3	13.34°	0.14	0.13	0.16
4	17.99°	0.555	0.31	0.42
5	22.71°	0.89	0.46	0.71
6	27.60°	0.66	0.45	0.85
7	32.72°	0.215	0.29	0.68
8	38.15°	0.05	0.15	0.47

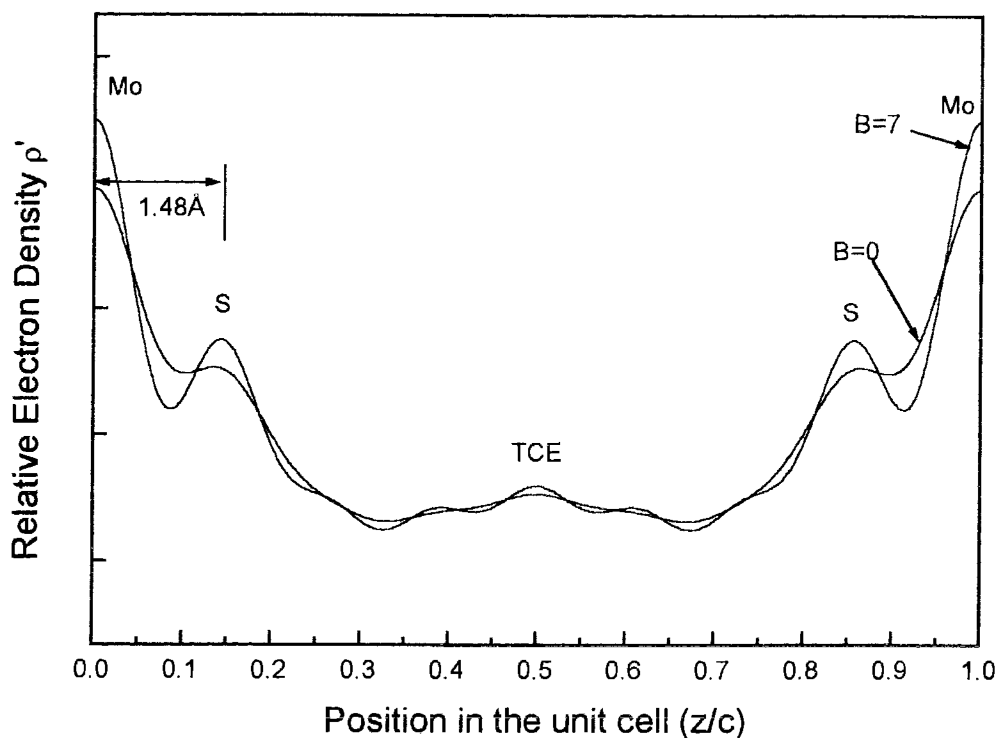

Fig.4.8 The relative electron density distribution along the c direction of an MoS_2/TCE film

The electron density distribution curve confirms that there is a single molecular layer of TCE between two adjacent MoS_2 layers in MoS_2/TCE system.

4.5. Calculating the MoS_2 basal plane orientation distribution of the Restacked MoS_2 film using the rocking curve experiments

With the Siemens D5000 diffractometer, the angle φ between the incident beam and the beam reaching the detector can be fixed and the X-ray tube and detector allowed to rotate together on the measuring circle while the sample is stationary (Fig. 4.9). When the angle φ is chosen such that the Bragg condition is satisfied for a certain set of lattice planes, i.e., $\varphi = \pi - 2\theta_B$, the resulting curve of X-ray intensity versus the angular position of the incident beam is called a rocking curve. With the rocking curve method, the diffraction angle θ_B is fixed, so the length of the scattering vector is a constant. The scattering vector **S** rotates while the angle of incident beam to sample surface changes.

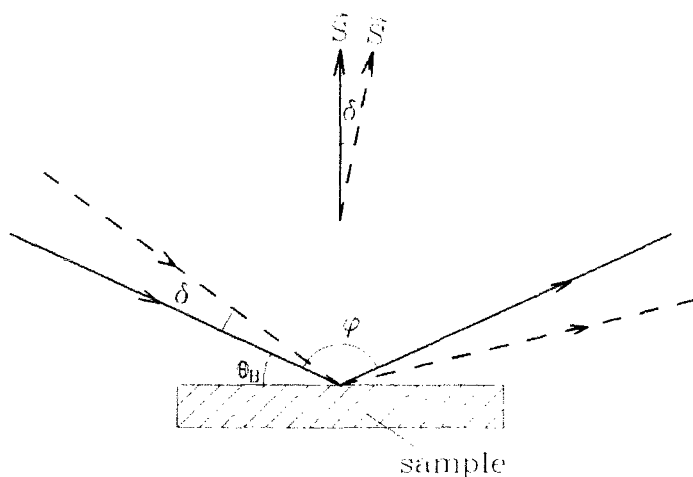

Fig.4.9 X-ray rocking curve measurement.
For a rocking curve measurement, the angle between the incident beam and the beam reaching the detector is fixed to $\varphi = \pi - 2\theta_B$ for a certain Bragg angle θ_B of the sample.

For a highly oriented system, only when the scattering vector is perpendicular to the set of lattice planes corresponding to the Bragg angle θ_B (constant at a particular value through out the measurement procedure), does the X-ray intensity reaches its maximum value. The

rocking curve for a highly oriented system appears as a peak. The more highly oriented the system is, the sharper the peak is. The half width of the peak provides the information about the degree of disorientation of that particular set of planes.

Here, we will use the rocking curve method to investigate the disorientation of the MoS_2 basal planes in a Restacked MoS_2 film which to a large degree reflects the orientation of the MoS_2/TCE film. The rocking curve measurements were done for both 2H-MoS_2 crystal powder and the Restacked MoS_2 film on the (002) line at $2\theta_B = 14.24°$. The experimental setups are identical for both measurements using the Siemens D5000 diffractometer with a 0.5° aperture diaphragm, a 1° scattered radiation diaphragm and without any detector diaphragm.

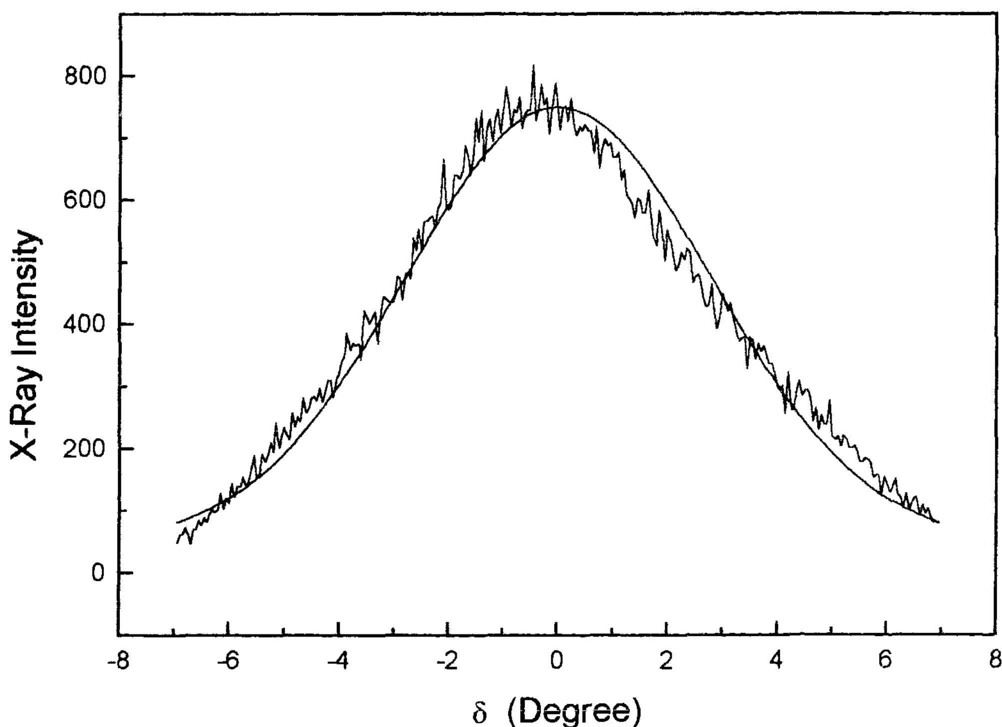

Fig.4.10 The rocking curve of the 2H-MoS_2 random oriented powder.
The X-ray intensity versus δ curve (the ragged line) is due to a geometric effect and it can be approximated by a Gaussian function (the smooth line).

Fig.4.10 is the rocking curve of $2H\text{-}MoS_2$ crystal random oriented powder. δ is the angular deviation of the scattering vector **S** from the normal of the sample surface.

Ideally, the rocking curve for a system of random oriented powder should show a constant X-ray intensity. However, the experimental rocking curve for the $2H\text{-}MoS_2$ powder is not a flat line. The X-ray intensity changes with the changing angular deviation δ. This is mainly due to the following geometric effect.

As shown in Fig.4.11, when the scattering vector S is perpendicular to the sample surface, i.e., $\delta = 0$, the sample is on the tangential plane of the focusing circle of the diffractometer. The area of the sample within the focused region reaches its maximum, so the X-ray intensity has the maximum value. When the scattering vector S rotates away from the normal of the sample surface, the sample surface is no longer on the tangential plane of the focusing circle, and the X-ray intensity will drop down due to the reduction of the focused sample area. Moreover, the asymmetric shape of the intensity curve is due to the changing cross-sections of the X-ray beams and a small factor of X-ray absorption.

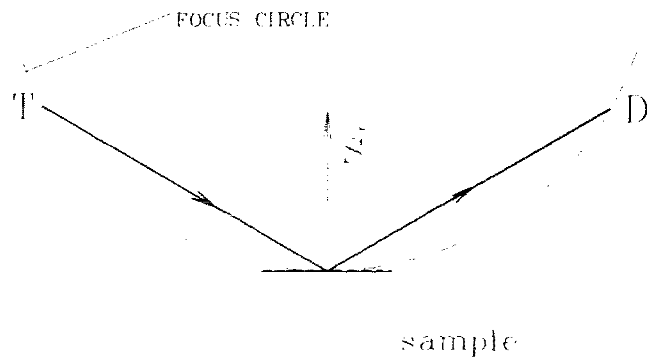

Fig.4.11 A geometric effect accompanying the rocking curve measurements is caused by the focus function of the diffractometer.

A Gaussian approximation can be used to formulate the intensity distribution due to the geometric effect. In Fig.4.10, the smooth line on top of the measured rocking curve corresponds to the Gaussian function:

$$I_g = I_{g0} e^{-\frac{\ln 2}{\alpha_g^2}\delta^2} \tag{4.8}$$

where I_{g0} is the maximum X-ray intensity and α_g is the half-width of the rocking curve of the $2H\text{-}MoS_2$ powder.

The rocking curve for a Restacked MoS_2 film is shown in Fig.4.12, where δ is the angular deviation of the scattering vector **S** from the normal of the sample film on the glass substrate.

The rocking curve of the Restacked MoS_2 film can also be described by Gaussian distribution function,

$$I = I_0 e^{-\frac{\ln 2}{\alpha^2}\delta^2} + D \qquad (4.9)$$

where D is associated to the background scattering of the glass substrate and α is the half-width of the Gaussian curve.

For the rocking curve of the Restacked MoS_2 film, the intensity is mainly

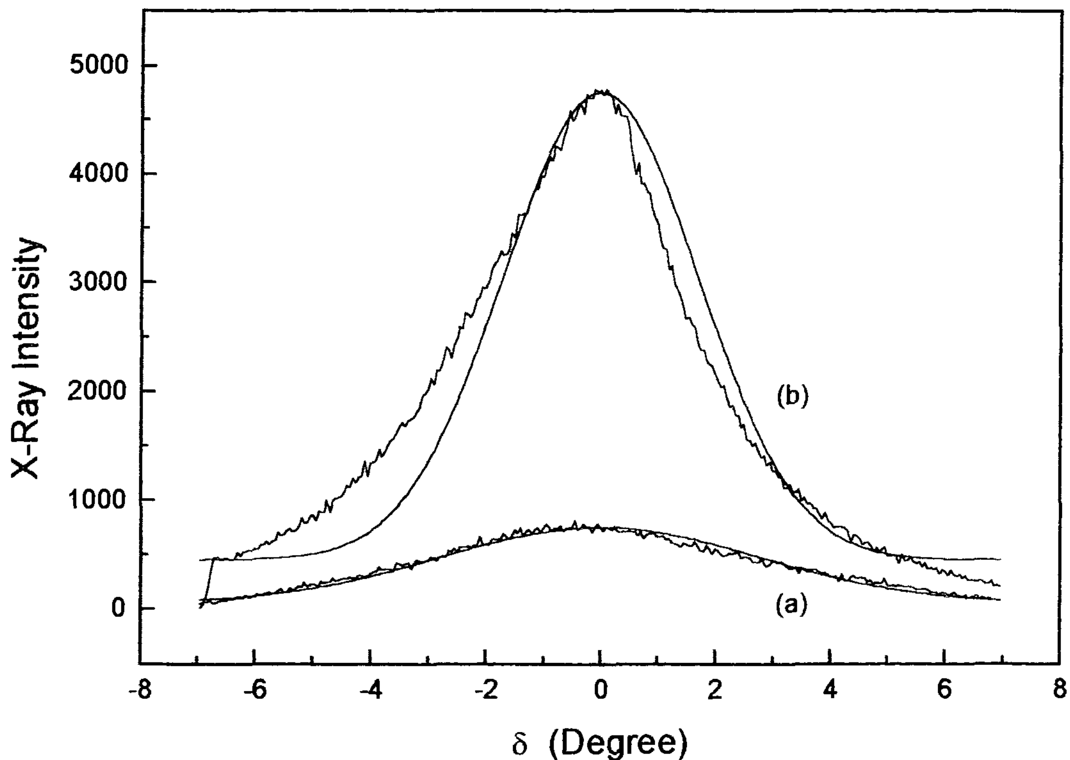

Fig.4.12 The rocking curve of the Restacked MoS_2 film.
(a) The rocking curve of the 2H-MoS_2 random oriented powder. It was used to represent the geometric effect; (b) The rocking curve of the Restacked MoS_2 film.
(The ragged lines are the experimental data and the smooth lines are the Gaussian approximations)

influenced by two factors. One is the geometric factor, $e^{-\frac{\ln 2}{\alpha_g^2}\delta^2}$. Another is the probability distribution of the MoS_2 basal plane orientation, P(δ). Therefore,

$$I = Ce^{-\frac{\ln 2}{\alpha_g^2}\delta^2} P(\delta) + D \tag{4.10}$$

From Equation (4.9) and (4.10), we get,

$$P(\delta) = Ae^{-\ln 2(\frac{1}{\alpha^2} - \frac{1}{\alpha_g^2})\delta^2} \tag{4.11}$$

where δ is the angular deviation of the MoS_2 basal plane from the sample surface.

Equation (4.11) shows that the most favorable orientation of the MoS_2 basal plane for Restacked MoS_2 film is parallel to the sample surface, i.e., the substrate. Also, the half-width of the orientation distribution curve, α_D, satisfies

$$\frac{1}{\alpha_D^2} = \frac{1}{\alpha^2} - \frac{1}{\alpha_g^2} \tag{4.12}$$

Using the experiment data, α_g = 3.3 ° and α = 2.0 ± 0.2 ° (the error results from the uncertainty in the background for the Gaussian fitting), we get α_D = 2.5 ± 0.5 °.

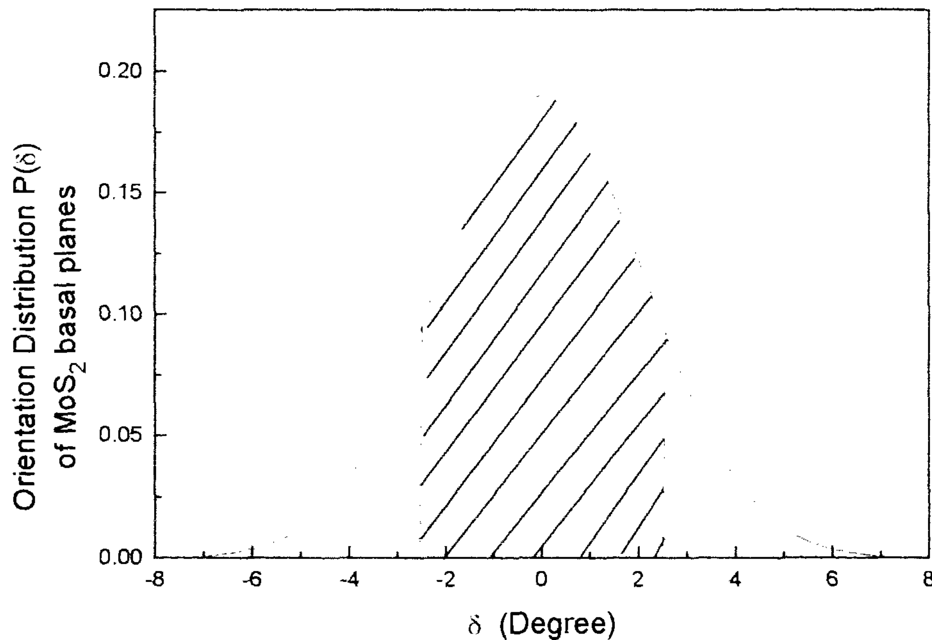

Fig.4.13 The orientation distribution of the MoS_2 basal planes in the Restacked MoS_2 film on glass substrate

The normalized orientation distribution curve for the Restacked MoS_2 film is plotted in Fig.4.13.

$$P(\delta) = Ae^{-\frac{\ln 2}{\alpha_D^2}\delta^2} \qquad (4.13)$$

in which A= 0.19.

Fig.4.13 shows that at least 70% of the total area of MoS_2 basal planes are oriented within ± 3 ° to the substrate surface.

Chapter 5
Optical Absorption and Electrical Resistance Measurements

Although the energy band structure of 1T–MoS_2 has not yet been calculated, Mattheiss's calculation[19] of the band structures of 1T-HfS_2, 1T-TaS_2, 2H-TaS_2, 2H-$NbSe_2$ and 2H-MoS_2 can be used to generalize the common features shared by all 1T polytypes or by all 2H polytypes of transition-metal-dichalcogenide layer compounds.

Mattheiss's results show the major difference in the d-band density of states between the octahedral and trigonal prismatic coordinations. In the octahedral phase (1T-MoS_2), the lower sub-band contains six states and the upper sub-band four states per

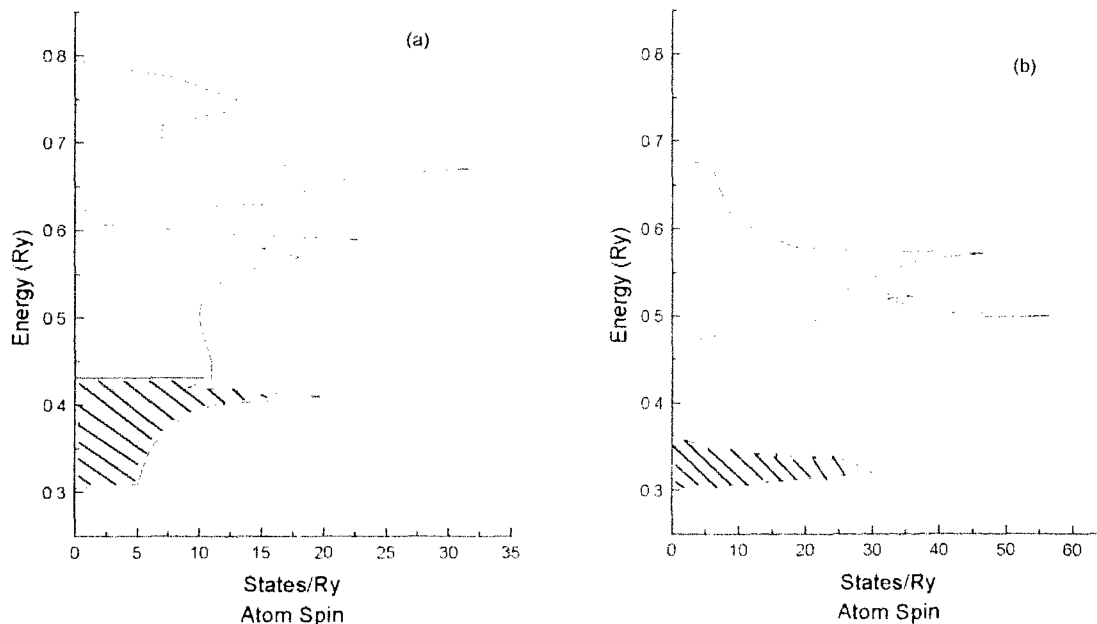

Fig.5.1 Comparison of d-band density of states for 1T-MoS_2 and 2H-MoS_2 based on Mattheiss's calculation
(a) a schematic diagram for 1T-MoS_2 .based on the result for 1T-TaS_2.
(b) a schematic diagram for 2H-MoS_2, the hatched region shows the occupied states

transition metal. Thus, 1T-MoS_2 would exhibit metallic behaviour since only two of the six states in the lower sub-band would be occupied. In the trigonal prismatic phase, a narrow d sub-band containing only two states is split off from the other eight states on the upper band by a gap of about 1.4 eV (see fig.5.1(b)). For 2H-MoS_2, the lower band is completely filled and the compound exhibits semiconducting behaviour. This major difference in d-band density of state is shown schematically in Fig.5.1, using 1T and 2H polytypes of MoS_2 as an example.

The analogy between 1T-TaS_2 and 1T-MoS_2 was first introduced by M. A. Py and R. R. Haering[4] to explain the driving mechanism for the trigonal prism to octahedral structural change upon Li intercalation of MoS_2. The band structure difference between the trigonal prism and octahedral coordinated MoS_2 has also been used to explain the electrical and optical properties of the sodium intercalated MoS_2[3] and the single-molecular-layer MoS_2[13].

In this chapter, optical absorption spectra and electrical resistance measurements of MoS_2/TCE and Restacked MoS_2 films will be presented.

5.1. Optical absorption spectra of MoS_2/TCE and Restacked MoS_2 films

The optical absorption spectra for MoS_2/TCE and Restacked MoS_2 films were obtained using a Hewlett Packard 8452A Diode Array Spectrophotometer. The optical spectra presented here are for two samples: O#1 is a MoS_2/TCE spread film on glass slide; O#2 is a Restacked MoS_2 film, which was obtained by heating O#1 in the vacuum environment at 250° for 17 hours.

Fig.5.2 shows the room temperature absorption spectra for samples O#1 and O#2. It is not surprising that the optical absorption for Restacked MoS_2 is similar to the one for

2H-MoS_2 crystal with a reduced intensity of all the absorption peaks, since in both systems the Mo atoms have trigonal prism coordination. The absorption peaks are associated with the band gap absorption as would be expected from Fig.5.1(b) where transitions between the filled band and empty higher bands give rise to strong absorption peaks labeled A and B in Fig.5.2. The spectrum for MoS_2/TCE does not show band gap absorption as might be expected from Fig.5.1(a) for MoS_2 with an octahedral coordination.

Thus the optical absorption results in Fig.5.2 indicate that MoS_2/TCE does not have the trigonal prism structure. This is in agreement with our X-ray diffraction results which indicate that in the transition from MoS_2/TCE to Restacked MoS_2 the Mo coordination undergoes a structural transformation from octahedral to trigonal prismatic.

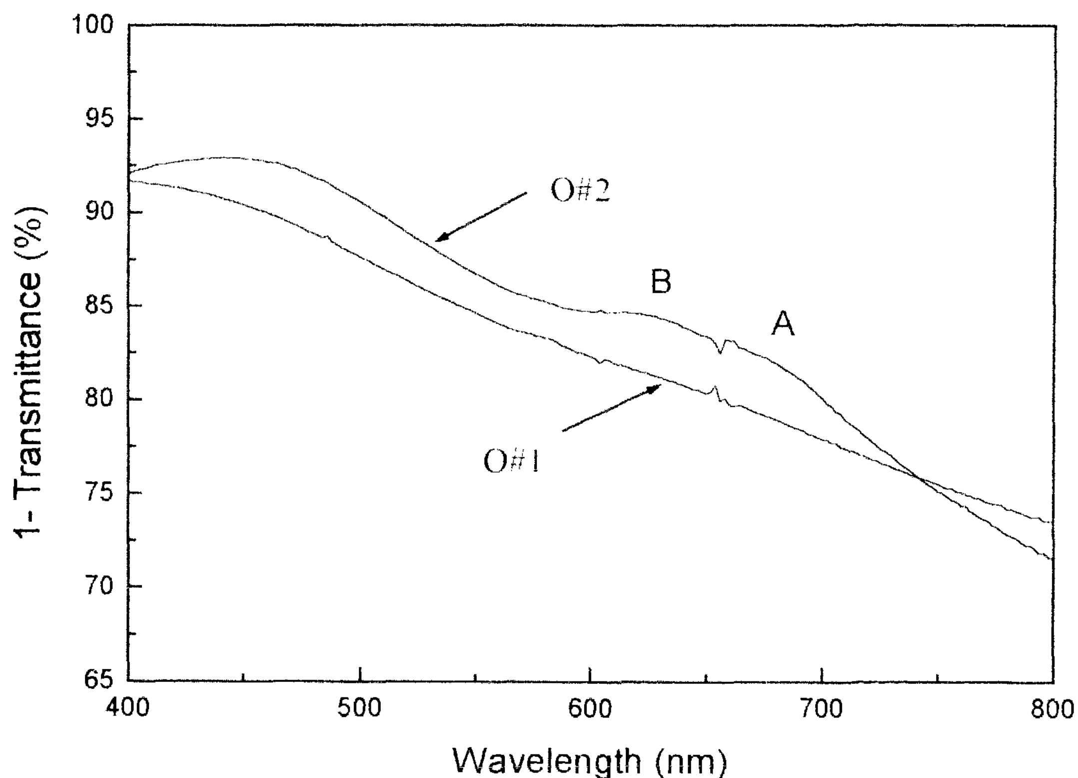

Fig.5.2 Room temperature optical absorption spectra of O#1 (MoS_2/TCE film) and O#2 (Restacked MoS_2 film)

5.2. Resistance vs. temperature measurement of MoS_2/TCE and Restacked MoS_2 systems

The resistance versus temperature measurement of MoS_2/TCE system was motivated by the results of Bissessur, et al. on the conductivity of $(PEO)_{0.92}MoS_2$[10]. $(PEO)_{0.92}MoS_2$ is a restacked MoS_2 system with poly-ethylene-oxide (PEO) included. The conductivity versus temperature measurement shows that a metal to insulator transition at 14-15K occurs in $(PEO)_{0.92}MoS_2$ which they attributed to charge density wave (CDW) formation. Their experimental results are shown in Fig. 5.3.

Despite many differences between the MoS_2/TCE system and the $(PEO)_{0.92}MoS_2$ system the two systems have a common feature: they are both organic inclusion MoS_2 systems. If the low temperature metal to insulator transition can be directly attributed to a structural phase transition of the MoS_2, the MoS_2/TCE system might also be a good

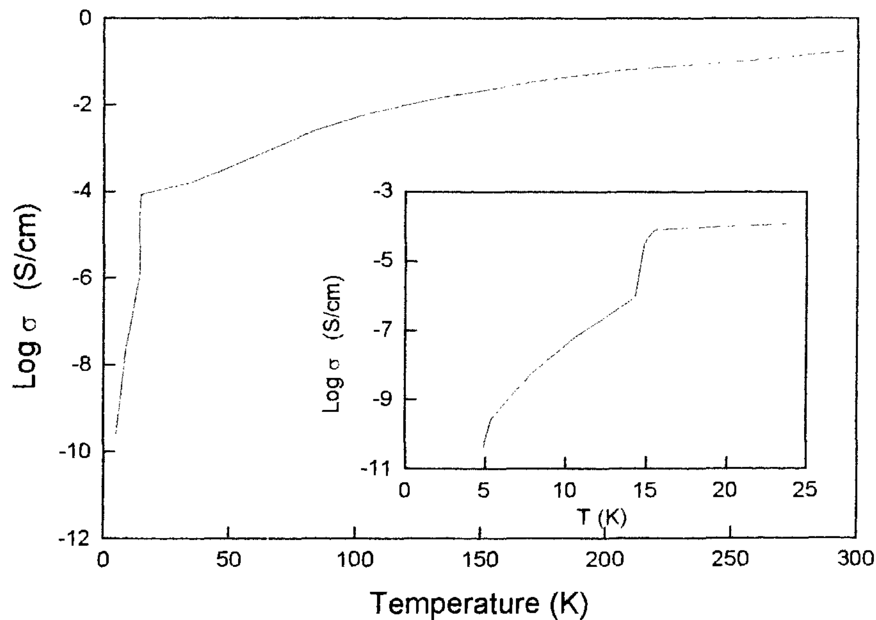

Fig.5.3 Four probe variable temperature electrical conductivity data for polycrystalline pellet of $(PEO)_{0.92}MoS_2$.
The metal to insulator transition is shown in more detail in the inset graph

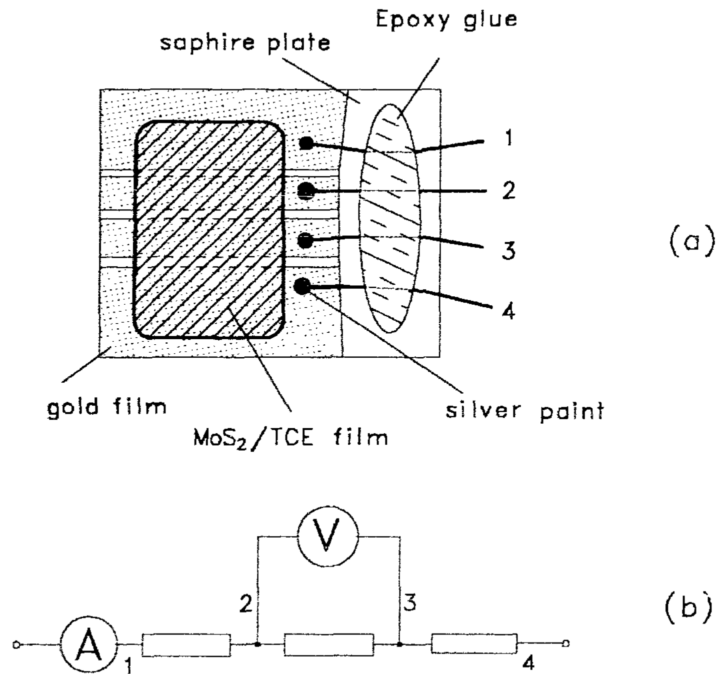

Fig.5.4 (a) The sample geometry for the four probe resistivity measurement; (b) The equivalent circuit

candidate for observing it.

For our resistance versus temperature measurements on MoS_2/TCE films, a four probe method was used. The sample geometry is shown in Fig.5.4 (a). Part of the sapphire plate was coated with a thin layer of gold. Three parallel lines were scored through the gold film. This forms four probes. The gaps between the probes are approximately 50 microns wide. The MoS_2/TCE film with an area of 1cm^2 was loaded on the top of the substrate, covering the three gaps and making contacts with the gold probes. The contacts between the copper wire and the gold film are made with silver paint. The wires are fixed to the sapphire plate using epoxy. The equivalent circuit is shown in Fig.5.4 (b). Thus the sample is prepared for the measurement.

Two kinds of cryogenic systems were used for the measurement. One was a Helium Dewer with a completely sealed sample dip. A chromel(P) versus gold-0.07

atomic percent iron thermocouple was used for temperature measurement. With this system, the temperature can be lowered down to 2K with a vacuum pump helping liquid helium reach its superfluid state. The other kind of cryogenic system used was the APCI Cryogenic Refrigeration System with an APD-F Temperature Indicator/Controller manufactured by Air Products and Chemicals, INC. The temperature can reach as low as 10K with sample loaded.

The resistance versus temperature measurements were repeated with several samples using both cryogenic systems. All measurements gave similar results. With the APCI Cryogenic Refrigeration systems, a sample was first cooled down from room temperature to 10K and then heated back up to room temperature. For the purpose of comparison, the measurement results are plotted to show the relation between the negative log R (the resistance), which is proportional to log σ (the conductivity), and temperature. The insertion in Fig.5.5 is part of the data from the measurement on a different MoS_2/TCE sample with the Helium Dewer.

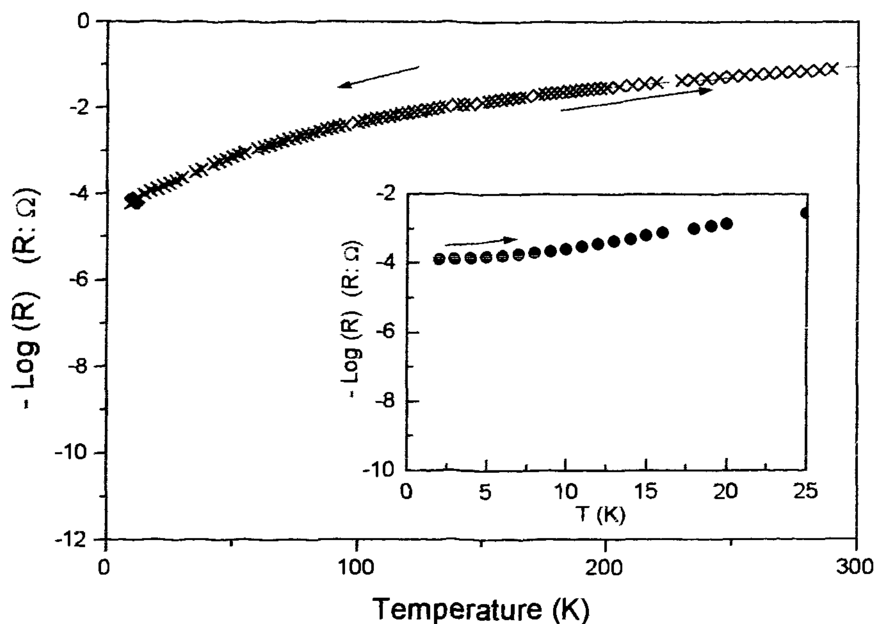

Fig.5.5 Resistance versus temperature data for MoS_2/TCE film using four probe geometry

Comparing Fig.5.5 with Fig.5.3, one can observe that from room temperature down to 50K, the MoS_2/TCE system and the $(PEO)_{0.92}MoS_2$ behave very similarly to each other as semimetals. However, no phase transition is observed for MoS_2/TCE system as for $(PEO)_{0.92}MoS_2$, which has a metal to insulator transition at 14-15K.

In order to observe the change of resistivity upon desorption of TCE from the MoS_2/TCE system, the MoS_2/TCE sample was heated up to 100°C. After being heated at 100°C overnight, the MoS_2/TCE system became a mixed phase of MoS_2/TCE and Restacked MoS_2. Fig.5.6 shows the temperature dependence of resistance for both systems. The measurement was done using the APCI Cryogenic Refrigeration System.

After all TCE molecules are driven out of the MoS_2/TCE system to form Restacked MoS_2/TCE, the resistance increases significantly. The resistance becomes more temperature dependent as is expected for a MoS_2 structural phase transition from octahedral in the MoS_2/TCE system to (semiconducting) trigonal prism in the Restacked MoS_2 system.

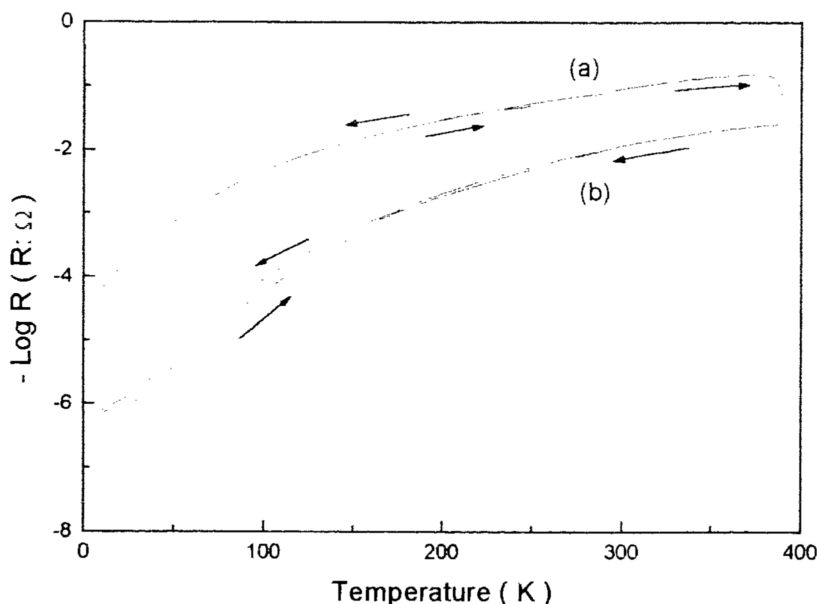

Fig.5.6 Resistance versus temperature data for: (a) MoS_2/TCE film and (b) a film with a mixed phase of MoS_2/TCE and Restacked MoS_2 (Arrows are used to indicate heating or cooling processes.)

Chapter 6
Conclusions

The structure of the restacked MoS_2 system with organic tetrachloroethylene (TCE) included, usually referred to as the MoS_2/TCE system, was studied using X-ray diffraction methods. It was found that the Mo coordination in MoS_2/TCE system is octahedral rather than trigonal prismatic as found in the original 2H-MoS_2 crystal.

With the X-ray reflection study, the thin and uniform MoS_2/TCE films are found to have a microscopic structure of single-molecular thick MoS_2 layers separated by one layer of TCE molecules and the film is an assembly of oriented crystallites with the MoS_2 basal planes highly parallel to the substrate. The near planar TCE molecules were found to be lying "flat" between MoS_2 layers providing the biggest contact area possible. Heating of the MoS_2/TCE facilitates the process of desorption of TCE to form Restacked MoS_2. From X-ray transmission on the oriented films and X-ray diffraction on the powder samples, it was found that when TCE was present the MoS_2 basal plane had an octahedral coordination and the MoS_2 layers are stacked turbostratically. When TCE was removed from the structure, the system tended to transfer back to the original 2H-MoS_2 which has a trigonal prismatic coordination, smaller interlayer spacing and ordered stacking.

The optical absorption spectrum and electrical resistivity measurements performed on MoS_2/TCE and Restacked MoS_2 films support the conclusion obtained from the X-ray studies that the Mo coordination is octahedral in MoS_2/TCE while it is trigonal prismatic in Restacked MoS_2. No evidance for any structural or phase transition was found in the electrical resistance of MoS_2/TCE down to 2K.

The important structural data and physical properties of MoS_2/TCE and Restacked systems are collected in Table 6.1.

The differing Mo coordination is the major factor contributing to the different optical and electrical performances of the material which has the MoS_2 layered structure as its frame. The results of our studies indicate that the Mo coordination is strongly related to the weak interaction between MoS_2 layers. However, the mechanism is still not clear at this stage and further studies are needed.

Table 6.1 Summary of structure parameters and physical properties of MoS_2/TCE and Restacked MoS_2 in comparison with 2H-MoS_2 crystal

	MoS_2/TCE	Restacked MoS_2	2H-MoS_2 crystal
interlayer spacing	10.00 ± 0.02 Å	6.22 ± 0.04 Å	6.17 Å
a-spacing	3.25 ± 0.02 Å	3.18 ± 0.02 Å	3.16 Å
superlattice	yes	no	no
Mo coordination	octahedral	trigonal prismatic	trigonal prismatic
stacking	turbostratic	partially ordered	ordered
optical absorption spectrum	no absorption peaks	band gap absorption observed	band gap absorption observed
electrical property	semimetal	semiconductor	semiconductor

Appendix
X-Ray Transmission Patterns for MoS_2/H_2O and Restacked MoS_2 Oriented Films

Since the MoS_2 water bilayer system (MoS_2/H_2O) has been studied extensively using X-ray powder diffraction method[7] and highly oriented thin MoS_2/H_2O film similar to MoS_2/TCE film is also easy to obtain, MoS_2/H_2O oriented film was chosen as the first object to which the X-ray transmission method was applied to test the applicability of the method.

A. Samples and substrate

The substrate is a thin, transparent plastic film—"Stretch & Seal" fixed on an aluminum frame.

Figure A.1 shows the results of the X-ray studies.

(a) is a MoS_2/H_2O film. This was made by releasing drops of MoS_2 single-layer water suspension onto the substrate. After the excess water had evaporated, a structure was formed in which MoS_2 basal planes were arranged parallel to the substrate and every single MoS_2 layers was separated from adjoining layers by two layers of H_2O molecules. The film had a dry appearance.

(b) is the film obtained by keeping the MoS_2/H_2O film (a) in a vacuum environment for 32 hours.

(c) is the film obtained by heating the film (b) in a vacuum environment for 2 hours at 60°C.

(d) is a Restacked MoS_2 film. This was obtained by heating the film (c) in a vacuum environment for 24 hours at 60°C.

B. Results and Comments

The X-ray transmission experiments were performed using Philips diffractometer. The aluminum frame which supports the substrate together with a lead mask restricts the sample examined to an area of 1(~2)mm $\times$10mm.

The X-ray transmission patterns are shown in Fig.A.1. The vertical lines mark the (100) and (110) peak positions of the 2H-MoS_2 crystal powder. The four peaks which come from the aluminum frame are marked "Al" and the unlabelled sharp small peaks

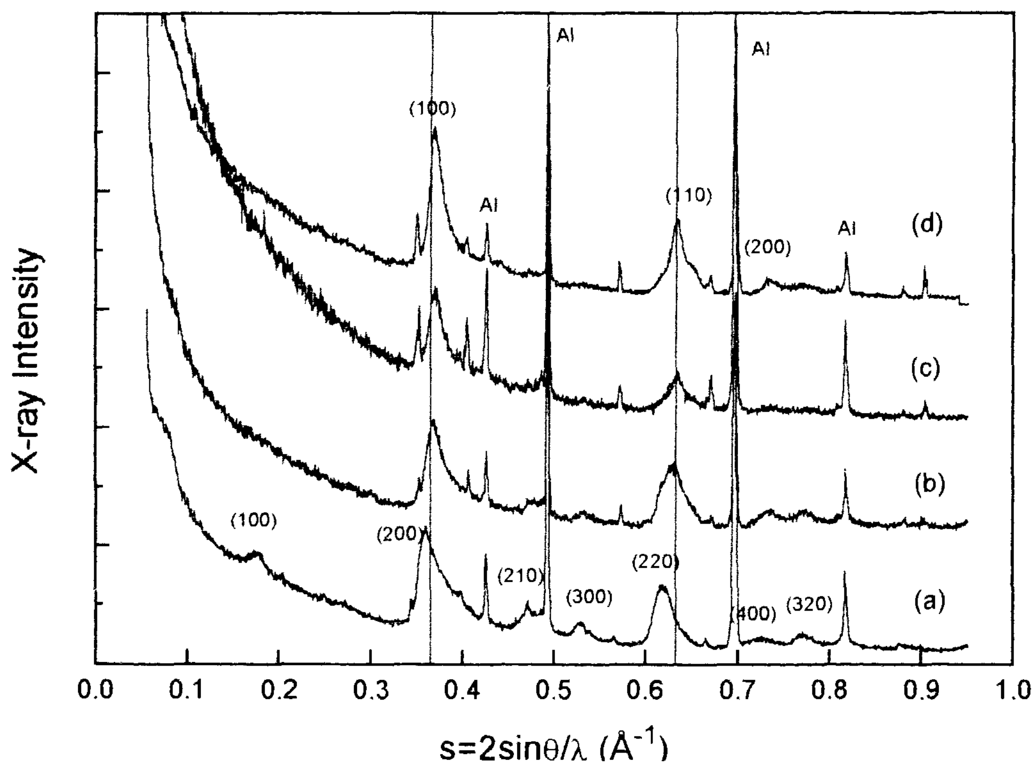

Fig.A.1 X-ray transmission patterns for MoS_2/H_2O and Restacked MoS_2 oriented films. (a) is a MoS_2/H_2O film; (b)&(c) are films with a mixed phase of MoS_2/H_2O and Restacked MoS_2; (d) is a Restacked MoS_2 film.

come from the lead mask.

The observation on the basal plane structure of MoS_2/H_2O is very similar to that of MoS_2/TCE. In MoS_2/H_2O, the MoS_2 layers are separated by water molecules. The Mo coordination is octahedral with a small distortion and an expanded a-spacing. This can be observed from the X-ray transmission pattern of MoS_2/H_2O compared to that of 2H-MoS_2, since the (200) and (220) peaks shifted to a lower angle which corresponds to an a-spacing of 3.25Å, 3% expansion from the a-spacing of 2H-MoS_2 crystal in which the Mo atoms are trigonal prismatically coordinated. The superlattice peaks, (100), (210), (300) and (320), are obvious in the X-ray transmission pattern which corresponds to a $2a_0 \times 2a_0$ superstructure as in MoS_2/TCE .

After the water molecules between the MoS_2 layers were removed and the Restacked MoS_2 film was formed, the (100) and (110) peaks shifted back to the peak positions of 2H-MoS_2 crystal and the superstructure was not observed. This indicates that the Mo coordination had transferred back to trigonal prism.

Neither (00l) lines nor (hkl) mixed lines were observed in the X-ray transmission patterns of MoS_2/H_2O and Restacked MoS_2. This is because the films are highly oriented.

The structural parameters obtained from the X-ray transmission patterns agree with the previous results[7] from the X-ray powder diffraction pattern of the MoS_2 water bilayer system. The X-ray transmission experiment on MoS_2/H_2O film provided a good example which shows that X-ray diffraction methods can be applied to investigate the basal plane structure of a highly oriented film.

Bibliography

1. Frindt, R. F., Phys. Rev., Vol. 140, No. 2A, A536-539, (1965).

2. Wypych, F. and Schollhorn, R., J. Chem. Soc., Chem. Commun., (1992), P1386-1388.

3. Acrivos, J. V., Liang, W. Y., Wilson, J. A. and Yoffe, A. D., J. Phys. Chem. 4, L18-20, (1971).

4. Py, M. A. and Haering, R. R., Can. J. Phys., Vol. 61, P76-84, (1983).

5. Chrissafis, K., Zamani, M., Kambas, K., Stoemenos, J., Economou, N. A., Samaras, I. and Julien, C., Mater. Sci. Eng., B3, P145-151, (1989).

6. Joensen, P., Frindt, R. F. and Morrison, S. R., Mat. Res. Bull., Vol. 21, P457-461, (1986).

7. Yang, D., Sandoval, S. Jimenez, Divigalpitiya, W. M. R., Irwin, J. C. and Frindt, R. F., Phys. Rev. B, Vol. 43, No. 14, P12053-12056, (1991).

8. Qin, X. R., Yang, D., Frindt, R. F. and Irwin, J. C., Ultramicroscopy 42-44, P630-636, (1992).

9. Divigalpitiya, W. M. R., Frindt, R. F. and Morrison, S. R., Science, Vol. 246, P369-371, (1989).

10. Bissessur, R., Schindler, J. L., Kannewurf, C. R. and Kanatzidis, M., Mol. Cryst. Liq. Cryst., Vol. 245, P249-254, (1994).

11. Gee, M. A., Frindt, R. F., Joensen, P. and Morrison, S. R., Mat. Res. Bull., Vol. 21, P543-549, (1986).

12. Kittel, C., *Introduction to Solid State Physics*, 6th Edition, P3-4.

13. Yang, Datong, *Powder Diffraction of Low Dimensional Materials and Properties of Single-Molecular-Layer* MoS_2, Ph.D. thesis, Simon Fraser University, (1993).

14. Alvarez, M., Bermejo, F. J., Chieux, P., Enciso, E., Alonso, J. and García, N., J. Condens. Matter, 1, P8595-8607, (1989).

15. D. Yang, private communication.

16. Stout, G. H. and Jensen, L. H., *X-Ray Structure Determination*, John Wiley & Sons, New York, (1989).
17. Lipson, H. and Taylor, C. A., *Fourier Transforms and X-Ray Diffraction*, G. Bell and Sons Ltd, London, (1958).
18. Cullity, B. D., *Elements of X-Ray Diffraction*, Addison-Wesley Publishing Company, Inc., Massachusetts, (1978).
19. Matteiss, L. R., Phys. Rev. B., 8, P3719-3740, (1973).